An extensive survey of phytoviral RNA 3' uridylation identifies extreme variations and virus-specific patterns

Anne-Caroline Joly, Shahinez Garcia, Jean-Michel Hily, Sandrine Koechler, Gérard Demangeat, Damien Garcia, Emmanuelle Vigne, Olivier Lemaire, Hélène Zuber, Dominique Gagliardi

An extensive survey of phytoviral RNA 3' uridylation identifies extreme variations and virus-specific patterns

Anne Caroline Joly[1], Shahinez Garcia[2], Jean-Michel Hily[2,3], Sandrine Koechler[1], Gérard Demangeat[2], Damien Garcia[1], Emmanuelle Vigne[2], Olivier Lemaire[2], Hélène Zuber[1,*] and Dominique Gagliardi[1,*]

[1]Institut de biologie moléculaire des plantes, CNRS, Université de Strasbourg, Strasbourg, France.
[2]UMR Santé de la Vigne et Qualité du Vin, INRAE, Université de Strasbourg, Colmar, France.
[3]Institut Français de la Vigne et du Vin, Le Grau-Du-Roi, France.

[*]Corresponding authors:
dominique.gagliardi@ibmp-cnrs.unistra.fr
helene.zuber@ibmp-cnrs.unistra.fr

The authors responsible for distribution of materials integral to the findings presented in this article in accordance with the policy described in the Instructions for Authors (https://academic.oup.com/plphys/pages/general-instructions) are: Dominique Gagliardi (dominique.gagliardi@ibmp-cnrs.unistra.fr), Hélène Zuber (helene.zuber@ibmp-cnrs.unistra.fr) and Emmanuelle Vigne (emmanuelle.vigne@inrae.fr).

Short title: Uridylation of phytoviral RNAs

Keywords
Uridylation, TUTase, RNA degradation, ssRNA phytovirus, TuMV, nepovirus, GFLV, grapevine

Abstract

Viral RNAs can be uridylated in eucaryotic hosts. However, our knowledge of uridylation patterns and roles remains rudimentary for phytoviruses. Here, we report global 3' terminal RNA uridylation profiles for representatives of the main families of positive single-stranded RNA phytoviruses. We detected uridylation in all 47 viral RNAs investigated here, revealing its prevalence. Yet, uridylation levels of viral RNAs varied from 0.2% to 90%. Unexpectedly, most poly(A) tails of grapevine fanleaf virus (GFLV) RNAs, including encapsidated tails, were strictly mono-uridylated, which corresponded to an unidentified type of viral genomic RNA extremity. This mono-uridylation appears beneficial for GFLV because it becomes dominant when plants are infected with non-uridylated GFLV transcripts. We found that GFLV RNA mono-uridylation is independent of the known TUTases HEN1 SUPPRESSOR 1 (HESO1) and UTP:RNA URIDYLYLTRANSFERASE 1 (URT1) in Arabidopsis (*Arabidopsis thaliana*). By contrast, both TUTases uridylate other viral RNAs like turnip crinkle virus (TCV) and turnip mosaic virus (TuMV) RNAs. Interestingly, TCV and TuMV degradation intermediates were differentially uridylated by HESO1 and URT1. Although the lack of both TUTases did not prevent viral infection, we detected degradation intermediates of TCV RNA at higher levels in a Arabidopsis *heso1 urt1* mutant, suggesting that uridylation participates in clearing viral RNA. Collectively, our work unveils an extreme diversity of uridylation patterns across phytoviruses and constitutes a valuable resource to further decipher pro- and anti-viral roles of uridylation.

Introduction

Viruses represent a constant threat to human health and food security worldwide. The development of effective antiviral strategies relies on understanding the molecular processes associated with the viral cycle and host-pathogen interactions. In plants, three main lines of defense have evolved to fight viral infections: physical barriers that viruses must overcome to penetrate into cells, the innate immune response and RNA silencing (Calil and Fontes, 2017). The RNA degradation machinery can also interfere with viral infections by adjusting the transcriptome and directly targeting viral RNAs. Recently, RNA uridylation was proposed as an antiviral defense mechanism in animals (Le Pen et al., 2018). RNA uridylation is the addition of one to several uridines at the 3' end of an RNA. This reaction is catalyzed by terminal uridylyltransferase (TUTases) and this post-transcriptional process is conserved across eucaryotes, except baker's yeast (*Saccharomyces cerevisiae*) (Scheer et al., 2016; De Almeida et al., 2018; Warkocki et al., 2018; Zigáčková and Vaňáčová, 2018; Yu and Kim, 2020). Uridylation targets both non-coding RNAs and mRNAs, and its primary ~~primordial~~ role is to induce RNA degradation (Scheer et al., 2016; De Almeida et al., 2018; Warkocki et al., 2018; Zigáčková and Vaňáčová, 2018; Yu and Kim, 2020). Interestingly, a genetic screen identified the TUTase COSUPPRESSION DEFECTIVE 1 (CDE-1) as a resistance factor for the Orsay virus (OrV) in *Caenorhabditis elegans* (Le Pen et al., 2018). CDE-1 was proposed to uridylate OrV RNA to facilitate its degradation. Similarly, TUT4 and TUT7, two cytosolic TUTases in human cells, repress the expression of influenza A virus mRNA and protein levels (Le Pen et al., 2018). Altogether, these observations led to the conclusion that RNA uridylation acts as an antiviral defense mechanism in animal cells (Le Pen et al., 2018).

Two TUTases have been characterized in Arabidopsis (*Arabidopsis thaliana*), HEN1 SUPPRESSOR 1 (HESO1) and UTP:RNA URIDYLYLTRANSFERASE 1 (URT1) (Ren et al., 2012; Sement et al., 2013), but their potential implication in 3′ terminal viral RNA uridylation has not been tested. Yet, U-tails and U-rich tails were detected on several full-length and truncated plant viral RNAs (Huo et al., 2016). However, this detection of viral RNA uridylation was restricted by the use of a low-throughput sequencing analysis of clones obtained by priming cDNA synthesis with an oligo(dA) primer, which cannot detect short uridine extensions. To obtain a large-scale view of phytoviral RNA uridylation as well as tailing by other nucleotides, we used 3'RACE-seq, a high-throughput sequencing strategy, to survey 3' nucleotide addition to viral RNAs from representatives of the main families of single-stranded positive (ss(+)) RNA viruses infecting plants. Our results reveal an unexpected diversity in phytoviral RNA uridylation patterns. We show that different activities, including the host TUTases URT1 and HESO1, can uridylate full-length viral RNAs but also truncated RNAs. The uridylation of truncated RNAs is a hallmark of degradation, suggesting that TUTases participate in the degradation of viral RNAs in plants, as it does for coding and non-coding RNAs. In line with this hypothesis, truncated turnip crinkle virus (TCV) RNA are detected at higher levels in a *heso1 urt1* mutant. We also identify that the poly(A) tails of both genomic RNAs of two nepoviruses, grapevine fanleaf virus (GFLV) and its closest relative arabis mosaic virus (ArMV), are mono-uridylated, thereby defining a hitherto unknown type of viral RNA 3' extremity. Mono-uridylation of GFLV RNAs becomes dominant in plants infected with non-uridylated transcripts. This *in vivo* optimization of GFLV RNA extremities indicates that the mono-uridylation of poly(A) tails is an intrinsic feature of GFLV RNAs that is likely advantageous for GFLV. In light of these results, we discuss the potential pro- and anti-viral roles of RNA uridylation.

Results

High resolution mapping of phytoviral RNA 3' ends by 3'RACE-seq

To explore the diversity of phytoviral RNA tailing, we initially selected 21 viruses representing 7 of the 8 orders of ss(+) RNA phytoviruses (Table 1). This selection of representative viral RNAs covers diverse types of phytoviral 3' extremities such as tRNA-like structures (TLS), various non-TLS 3' terminal structures and poly(A) tails. Because poly(A) tails can be either encoded or extended by poly(A) polymerases, we refer hereafter to 3' tailing as for the addition of nucleotides 3' to the poly(A) tail itself, irrespective of the mode of synthesis of the poly(A) tail.

Some of these 21 viruses have multipartite genomes and overall, 31 viral RNAs were analyzed by 3'RACE-seq (Table 1). A flow-chart showing all steps of the 3'RACE-seq protocol and of the bioinformatic analysis pipeline are available in (Scheer et al., 2020) and at https://github.com/hzuber67/RACEseq_virus, respectively. The Illumina-based 3'RACE-seq protocol allows for in-depth mapping of RNA 3' extremities with single nucleotide resolution, including the identification of any untemplated nucleotides. Of note, Unique Molecular Identifiers (UMIs) are incorporated by ligating the 3' ends of RNAs to an adapter that contains a 15-nucleotide degenerate sequence (see Supplemental Data Set S1 for information on all primers used in this study). This molecular barcoding allows for a deduplication step during data analysis and therefore each final read

corresponds to a single original RNA molecule. 3'RACE-seq has a few technical limitations that are worth to note in the context of this study. The first one is that 3'RACE-seq interrogates 3' extremities independently of 5' extremities and therefore, full-length viral RNAs and subgenomic RNAs sharing identical 3' extremities are not discriminated here. Also, the 3' ends of the RNA targets must be accessible to the T4 RNA ligase used to ligate the adapter. Therefore, certain modifications of the last nucleotide, like aminoacylation, will prevent ligation. Yet, the fraction of non-aminoacylated viral RNAs can still be analyzed. Finally, 3' terminal secondary structures may also impede T4 RNA ligase. To limit this effect, non-polyadenylated viral RNAs were briefly denatured at high temperature before the ligation step. Despite these few constraints, 3'RACE-seq remains a powerful method to accurately map 3' extremities of target RNAs.

The expected 3' ends and polyadenylated/non-polyadenylated statuses were confirmed for 19 out of the 21 viruses. However, the 3' terminal features of both grapevine leafroll-associated virus 2 (GLRaV-2, *Closteroviridae* family, *Closterovirus* genus) and carrot necrotic dieback virus (CNDV, *Secoviridae* family, *Sequivirus* genus) RNAs were reassessed. Unlike the viral RNAs of other members of the *Sequivirus* genus, the CNDV RNA was proposed to be polyadenylated because its 3' region could be amplified by RT-PCR using oligo(dT)-primed cDNA (Menzel and Vetten, 2008). It is possible that such an amplification was due to a minor fraction of CNDV RNA being polyadenylated or because this viral RNA ends with an A-rich region. However, our 3'RACE-seq data demonstrate that its 3' extremity is not constitutively polyadenylated. Indeed, 99.8% of the reads that map to the last nucleotide of the CNDV reference sequence are not tailed (Figure 1, A and B, Supplemental Data Set S2 and Supplemental Data Set S3). The CNDV RNA will therefore be classified amongst the non-polyadenylated viral RNAs hereafter in this study.

The current description of the 3' terminal features of the GLRaV-2 RNA is rather contradictory. The GLRaV-2 RNA is described as not polyadenylated by several resources gathering general information on viruses, like the International Committee on Taxonomy of Viruses (ICTV) or ViralZone (Hulo et al., 2011). Yet, several GLRaV-2 RNA sequences ending with either a short poly(A) tail or a longer A-rich region followed by a short nucleotides stretch like GAAGC or GCGGCCGC have been reported (Zhu et al., 1998; Liu et al., 2009). Our 3'RACE-seq experiment revealed that most (90.4%) of GLRaV-2 RNA 3' ends correspond to A-rich tails, *i.e.* heteropolymeric tails containing a majority of As (Figure 1 C to E, Supplemental Data Set S2 and Supplemental Data Set S3). Only a minority (8.7%) of these tails are homopolymeric which is in contrast to the pure adenosine extensions of 8 other selected viruses whose RNAs are polyadenylated. A sequence logo analysis indicates that A-rich tails often terminate with GAAGC, as previously reported for a GLRaV-2 infectious clone (Liu et al., 2009) (Figure 1F). Overall, our 3'RACE-seq analysis shows that GLRaV-2 RNAs have complex 3' A-rich tails. It is likely that homopolymeric poly(A) tails and A-rich tails of phytoviral RNAs are produced by different enzymes or distinct mechanisms yet to be elucidated. However, it is unknown at present whether they would entail different functions. In any case, GLRaV-2 RNA is considered hereafter in a specific sub-class of polyadenylated viral RNAs with A-rich tails.

Extreme diversity of RNA uridylation levels across ss(+) RNA phytoviruses

The diversity of 3' terminal nucleotide addition was then analyzed for the 21 selected viruses. Three main observations were made. Firstly, 3' tailing of plant viral RNAs is pervasive. Overall, viral RNAs can be adenylated, cytidylated, guanylated, uridylated or tailed with mixed nucleotide extensions (Figure 2A, Supplemental Figure S1, Supplemental Data Set S2 and Supplemental Data Set S3). Secondly, an extreme variability in uridylation levels was detected for viral RNAs, ranging from 0.2% to 90% (Figure 2A). Of note, we cannot exclude that the smallest level of uridylation detected for CNDV RNA may correspond to background level, with no biological importance. Also, these percentages refer to uridylation detected by 3'RACE-seq in the 3' most terminal region of viral RNAs and additional upstream uridylation sites may also exist but are not considered here. The third and last general observation is that 3' terminal uridylation patterns are heterogeneous, from strict mono-uridylation for some viral RNAs to tails up to 30 uridines, which is the maximal size measured with our analysis pipeline (Figure 2B, Supplemental Data Set S3C). This striking variability in uridylation levels and patterns likely indicates distinct roles in viral RNA metabolism. We therefore decided to focus our study on further analyzing phytoviral RNA uridylation.

Extreme diversity of uridylation patterns for polyadenylated phytoviral RNAs

One of the most striking findings from our large survey of phytoviral RNA tailing was the unexpected amplitude of 3' terminal uridylation levels among phytoviral RNAs that are polyadenylated (Figure 2A). The selected viruses with polyadenylated genomic RNAs correspond to grapevine fanleaf virus (GFLV), potato virus X (PVX), grapevine red globe virus (GRGV), grapevine rupestris stem pitting-associated virus (GRSPaV), grapevine Pinot gris virus (GPGV), grapevine virus B (GVB), turnip mosaic virus (TuMV), beet necrotic yellow vein virus (BNYVV) and grapevine leafroll-associated virus 2 (GLRaV-2) (see classification in Table 1).

As compared to GFLV RNAs, all other polyadenylated viral RNAs analyzed here are uridylated to a modest extent averaging 4% (Figure 2A). In addition, those RNAs can be uridylated by one to several uridines (Figure 2B) and the uridylated poly(A) tails are significantly shorter as compared to non-uridylated ones (Figure 3). All these features are fully reminiscent of the uridylation characteristics previously reported for mRNAs in Arabidopsis (Morozov et al., 2012; Sement et al., 2013; Zuber et al., 2016; Scheer et al., 2021). By contrast, GFLV RNA uridylation patterns have three remarkable features as compared to mRNAs and all other polyadenylated viral RNAs investigated here. Firstly, GFLV RNAs are uridylated to very high levels (>81%) (Figure 2A). The high uridylation level of both GFLV RNAs is not host-specific because similar uridylation levels were detected when Arabidopsis and quinoa (*Chenopodium quinoa*) were used as hosts (compare Figure 2A, Figure 4A and Figure 8A). Secondly, GFLV RNAs are strictly mono-uridylated (Figure 2B, Figure 4B and Figure 8A), and thirdly, uridylated and non-uridylated GFLV poly(A) tails have similar sizes (Figure 3). To our knowledge, no other RNA has a similar uridylation pattern in plants.

Unique high uridylation rates of GFLV and ArMV among *Secoviridae*

Two members of the *Secoviridae* family, CNDV and GFLV, were among the initial selection of viruses analyzed in Figure 2. Yet, those viral RNAs have contrasting features. The single CNDV RNA

is not polyadenylated and hardly uridylated, whereas both GFLV RNAs are polyadenylated and uridylated to high levels. To evaluate the evolutionary conservation of GFLV 3' terminal features among *Secoviridae*, we selected 8 other representatives of this family. Those viruses are cowpea mosaic virus (CPMV), broad bean wilt virus 1 (BBWV-1), raspberry ringspot virus (RpRSV), tobacco ringspot virus (TRSV), arabis mosaic virus (ArMV), tomato black ring virus (TBRV), cherry leaf roll virus (CLRV) and strawberry latent ringspot virus (SLRSV) (see Table 2 for classification and RNA 5' and 3' terminal features). Except for CNDV, all other selected *Secoviridae* including GFLV have two genomic RNAs, that are described as polyadenylated. The evolutionary relationship between these viruses is illustrated by a phylogenetic tree built using the amino acid sequence of the conserved protease-polymerase (Pro-Pol) region used by ICTV to define *Secoviridae* species (Figure 4A, Supplemental Figure S2). Remarkably, only GFLV and ArMV RNAs share a much higher level of mono-uridylation among the *Secoviridae* (Figure 4). In fact, even among the 6 selected members of the *Nepovirus* genus, the high level of mono-uridylation is unique to GFLV and ArMV RNAs, as the 4 other nepovirus RNAs are uridylated to low levels (<1.2%) as compared to GFLV and ArMV RNAs (Table 2, Figure 4). Therefore, an extreme diversity of uridylation patterns of viral RNAs can occur even within a genus.

Phytoviral RNAs with a TLS are poorly uridylated

To pursue our description of phytoviral RNA uridylation, we then analyzed the uridylation patterns of 18 non-polyadenylated viral RNAs from 12 phytoviruses (see Table 1 for genomic features). Those phytoviral RNAs are uridylated from 0.2% up to ca 10% (Figure 2A). Seven of the 12 selected phytoviruses have a relatively low level of uridylation (<2.2%): peanut clump virus (PCV), cucumber mosaic virus (CMV), turnip yellows virus (TuYV), tobacco mosaic virus (TMV), alfalfa mosaic virus (AlMV), turnip yellow mosaic virus (TYMV) and CNDV (see classification in Table 1). Interestingly, four of these seven viruses have a known 3' terminal TLS that can be aminoacylated: PCV, CMV, TMV and TYMV (Dreher, 2010). Aminoacylation will prevent uridylation, and the extent of the competition between uridylation and aminoacylation is difficult to estimate *in planta*. Yet, among those viral RNAs that remain not aminoacylated *in vivo*, and therefore detectable by 3'RACE-seq, only a minor proportion is uridylated (from 0.3 to 2.2 %) (Figure 2A). Hence, those TLS seem to be poor substrates or poorly accessible to the enzymatic activities responsible for uridylating viral RNAs.

The three other viral RNAs with a low level of uridylation are the TuYV, CNDV and AlMV RNAs. To our knowledge, the structure of the 3' terminal region has not been determined for TuYV and CNDV RNAs. By contrast, the 3' terminal region of AlMV RNA is known to switch between two alternative conformations (Olsthoorn et al., 1999). Either five 3' terminal stem-loop structures bind the coat protein favoring translation, or a pseudoknot allows a conformational rearrangement to generate a structure resembling a TLS and this pseudoknot is necessary for replication (Olsthoorn et al., 1999). This TLS-like conformation, but also probably the binding of the coat protein, may restrict access to uridylating activities, thereby explaining the low uridylation rate of the three AlMV RNAs (Figure 2A).

Uridylation of degradation intermediates reveals patterns of ribonucleolytic attacks

The five other phytoviruses with non-polyadenylated RNAs have a relatively higher level of uridylation, from 3.4 to 12 % (Figure 2A): grapevine leafroll-associated virus 1 (GLRaV-1), turnip crinkle virus (TCV), sowbane mosaic virus (SoMV), tomato bushy stunt virus (TBSV), and tobacco rattle virus (TRV) (see classification in Table 1). SoMV and TRV RNAs are uridylated mostly at their mature extremities, similarly to what is observed for the TLS-ending RNAs of PCV, CMV, TMV and TYMV, and for the three AlMV RNAs (Figure 5A, Supplemental Figure S3). Therefore, the higher uridylation rates for SoMV and TRV RNAs as compared to viral RNAs ending with a TLS likely reflect a greater accessibility of their 3' extremities by TUTase(s) or alternatively, a higher stability of those RNAs even when uridylated. Yet, the accessibility of the 3' terminal extremities is not the only feature regulating uridylation as we also detected uridylation sites located upstream of mature 3' extremities. Some of these internal uridylation sites are not conserved between replicates as for PCV RNA1 and RNA2, or are scarce as for SoMV and TuYV RNAs (Figure 5A, Supplemental Figure S3). By contrast, robust uridylation patterns of truncated viral RNAs that are well conserved across biological replicates were identified for TBSV, TCV and GLRaV-1 RNAs (Figure 5A). Because of the internal position of these uridylation sites and the current knowledge of the primordial role of uridylation in triggering RNA degradation in the cytoplasm of eukaryotes, including Orsay virus (OrV) RNAs in *C. elegans* (Le Pen et al., 2018), we propose that these truncated uridylated viral RNAs represent degradation intermediates.

The GLRaV-1 RNA displays some ragged 3' extremities in a ca 100 nt window upstream of its major 3' extremity and those extremities correspond to the main uridylation sites (Figure 5A). It is therefore possible that GLRaV-1 RNA 3' extremities are subjected to repeated cycles of uridylation and exoribonucleolytic nibbling to overcome stabilizing bound proteins or structural elements. To our knowledge, such features are not yet been characterized for GLRaV-1. By contrast, the structure of the TCV RNA 3' region has been studied intensively. The TCV RNA 3' UTR begins with a region of ca 50 nt that was first termed the unstructured region (USR) albeit it was later shown to contain a weakly structured hairpin, named M3H (Yuan et al., 2012; Simon, 2015). Immediately downstream of USR/M3H are five stable hairpins (H4, H4a, H4b, H5 and Pr) and three H-type pseudoknots (Ψ1, Ψ2, Ψ3) (McCormack et al., 2008; Simon, 2015). The pseudoknots H4a/ Ψ3 and H4b/ Ψ2 together with H5 fold into a T-shaped structure (TSS) (Le et al., 2017) (Figure 5B). The strong structure of the TCV RNA 3' region clearly influences its uridylation pattern: three highly reproducible clusters of uridylation sites are detected within the last 200 nt (Figure 5B). Cluster I corresponds to the USR/M3H region which is positioned exactly upstream of the H4 hairpin. Cluster II corresponds to the loop of H4b hairpin and cluster III to the 3' most terminal 5 nucleotides (UGCCC) of TCV that are immediately downstream of the G/C-rich Pr hairpin. Those terminal nucleotides are likely either directly accessible to the uridylating activities or generated by nibbling of mature 3' extremities up to the Pr hairpin. Very few uridylation sites are detected between the three clusters suggesting that hardly any degradation intermediates are generated in those regions. Rather, the clusters of uridylation sites upstream of H4 and in the H4b loop indicate that these sites could correspond to 3' extremities of degradation intermediates.

Because of their robustness across biological replicates, the uridylation patterns of TBSV, TCV and GLRaV-1 RNA degradation intermediates represent signatures of either endoribonucleolytic or 3'-5' exoribonucleolytic attacks that generate truncated RNAs. Those signatures contribute to understanding 3'-5' degradation processes of phytoviral RNAs, especially in light of structural data of their 3' region. Of note, the three uridylation clusters detected when TCV infects *Nicotiana benthamiana* are also detected in Arabidopsis (Supplemental Figure S4). However, the positions of the main uridylation sites are shifted in the clusters I and III (Supplemental Figure S4). Hence, the degradation signatures of TCV RNA vary between the two host plant species, likely reflecting differences in RNA degrading activities. For instance, the Arabidopsis Col-0 genetic background used in this study lacks an active 3'-5' exoribonuclease called SUPPRESSOR OF VARICOSE (SOV) (Zhang et al., 2010), the plant ortholog of DIS3 Like 3'-5' Exoribonuclease 2 (DIS3L2), which preferentially degrades uridylated RNAs (Malecki et al., 2013; Faehnle et al., 2014).

Known host TUTases differentially uridylate TuMV and TCV RNAs

The characteristic uridylation patterns of TCV and TuMV RNAs make those viral RNAs adequate models to test whether and which TUTases of the host plant are responsible for uridylation of non-polyadenylated and polyadenylated viral RNAs. Two TUTases have been characterized in Arabidopsis, URT1 and HESO1 (Ren et al., 2012; Sement et al., 2013). Although both enzymes may cooperate in uridylating common RNA substrates, they have marked preferences: URT1 is the main TUTase uridylating mRNAs, whereas HESO1's main substrates are small RNAs and RISC-cleaved mRNAs (Ren et al., 2012; Zhao et al., 2012; Sement et al., 2013; Tu et al., 2015; Zuber et al., 2016; Zuber et al., 2018; Scheer et al., 2021). HESO1 was proposed to synthesize longer tails than URT1 (Tu et al., 2015). Longer tails may be U-rich rather than homopolymeric, because some TUTases may infrequently incorporate A, G or C. Because U-rich tails were detected on TCV RNA (Supplemental Figure S1C), we first compared the profiles for both only-U and U-rich tails after TCV infection of wild-type (Col-0) plants, the *urt1-1* and *heso1-4* single mutants, as well as the double mutant *heso1-4 urt1-1*. The only-U and U-rich tails were detected at similar positions in wild-type Arabidopsis (Figure 6, B to E).

Interestingly, while only-U tails slightly decrease in the *heso1-4* mutant, U-rich tails drastically drop in *heso1-4*, demonstrating that HESO1 uridylates TCV RNA and has a predominant role in the addition of U-rich tails (Figure 6, A to D). TCV RNA uridylation is abrogated in the double mutant *heso1-4 urt1-1*, indicating that URT1 can also uridylate TCV RNA. Yet, URT1 and HESO1 are not fully redundant because distinct 3' extremities were uridylated in the respective *urt1-1* and *heso1-4* single mutants (Figure 6, B to D). For instance, the 3' terminal uridylation (cluster III) is unchanged in the *urt1-1* mutant as compared to wild type, but almost abrogated in the *heso1-4* mutant (Figure 6D). Therefore, the 3' terminal uridylation of TCV RNA is mostly catalyzed by HESO1. Conversely, URT1 preferentially uridylates some positions in clusters I and II (Figure 6, B and C). In most cases, URT1 uridylates TCV RNA 3' extremities terminating by As, whereas HESO1 seems to prefer 3' extremities ending with non-A nucleotides (Figure 6E). This differential uridylation of TCV RNA by both TUTases actually reflects their known *in vitro* and *in vivo* substrate specificities (Sement et al., 2013; Tu et al.,

2015). TCV can infect both the *urt1-1* and *heso1-4* single mutants, as well as the *urt1-1 heso1-4* double mutant (Supplemental Data Set 2e), indicating that both TUTases are not limiting factors for TCV infection of Arabidopsis of the Col-0 accession. Yet, TCV RNA degradation intermediates accumulate to higher levels in the double mutant *heso1-4 urt1-1* (Figure 6F). This increased accumulation shows that both URT1 and HESO1 participate in the degradation of TCV RNA even though both TUTases are not essential to restrict infection by TCV.

The respective involvement of URT1 and HESO1 in uridylating a polyadenylated phytoviral RNA was then tested using TuMV RNA. Uridylation levels significantly drop in a *urt1-1* mutant but not in a *heso1-4* mutant, indicating that URT1 has a predominant role in uridylating TuMV RNA (Figure 7A). Yet, uridylation is almost abrogated in the double mutant *heso1-4 urt1-1*, revealing a secondary role for HESO1. Interestingly, the median of U-tail sizes was significantly decreased in the *heso1-4* mutant while increased in the *urt1-1* mutant (Figure 7B). These results show that HESO1 adds longer tails than URT1 to TuMV RNA, as previously proposed for miRNAs (Tu et al., 2015). Another notable difference was that the oligo(A) tails uridylated by HESO1 are shorter than for URT1 (Figure 7, C and D). The median sizes of oligo(A) tails uridylated in wild type and in the *heso1-4* mutant are 10 and 11 nt, respectively, whereas this size drops to 4 nt when only HESO1 uridylates TuMV oligo(A) tails in the *urt1-1* mutant. This difference in uridylated oligo(A) tail size suggests a sequential action of both TUTases.

Altogether, those data reveal viral RNAs as RNA substrates shared by both URT1 and HESO1, albeit with different preferences for uridylation sites and tail composition. Even though TUTases cannot prevent infection, these data indicate that the 3' extremities of viral RNA degradation intermediates are accessible to TUTases, which participate in the process of viral RNA degradation.

GFLV RNAs are not uridylated by known host TUTases

By contrast to TCV and TuMV RNAs, the atypical mono-uridylation pattern of GFLV RNAs did not support the involvement of neither URT1 nor HESO1. Indeed, the lack of either URT1, HESO1 or both TUTases did not affect the high uridylation level of both GFLV RNAs (Figure 8A, Supplemental Figure S5). Knowing whether the atypical mono-uridylation of GFLV RNA1 and RNA2 is also shared by their respective negative strands may contribute to understanding the GFLV RNA mono-uridylation process. We therefore mapped the 3' end of both negative strands of GFLV RNA1 and RNA2 by 3'RACE-seq. For both negative strands, most reads (70.1%) map to the expected 3' terminal nucleotide, which is a uridine (Figure 8B). This 3' terminal uridine of both minus strands is complementary to the previously mapped 5' terminal adenosine of each positive strand (Serghini et al., 1990; Ritzenthaler et al., 1991; Vigne et al., 2013; Martin et al., 2021). Therefore, the 3' terminal uridine of GFLV negative strand is encoded.

To check whether the poly(A) tail and 3' terminal uridine of the positive strands are encoded as well, the 5' extremity of each negative strand was mapped. Those extremities are not accessible to ligation, presumably because of the presence of a viral protein genome-linked (VPg). Therefore, a complementary DNA strand was synthesized to each RNA negative strand, and the cDNA 3' extremities were mapped by an adapted RACE-seq protocol (Supplemental Figure S6A). The 5'

extremities of RNA1 and RNA2 positive strands were simultaneously mapped as controls. The RACE-seq results confirmed the 5' extremity of both positive strands as previously reported (Serghini et al., 1990; Ritzenthaler et al., 1991; Vigne et al., 2013; Martin et al., 2021), validating the experimental approach (Supplemental Figure S6B). Interestingly, oligo(U) of up to 50 Us were detected as 5' sequences of both RNA1 and RNA2 negative strands (Figure 8B). However, a terminal adenosine 5' to the oligo(U) was never observed for the negative strands which would have indicated that the 3' terminal uridine of the positive strands is encoded by the minus strand.

Overall, our data show that uridylation of GFLV viral genomic RNAs is independent of the host TUTases, URT1 and HESO1, and that both negative and positive GFLV RNA1 and RNA2 strands terminate with a 3' uridine. In addition, our results indicate that the 3' terminal uridine of the negative strands is encoded by the 5' terminal adenosine of the positive strands and that at least part of the poly(A) tail of the positive strands is encoded by oligo(U) sequences of the negative strands. Even if a negative result cannot be interpreted as proof, we could not find evidence that the 3' terminal uridine of the positive strands is encoded by the minus strand. Therefore, either this uridine is added by a yet unknown terminal nucleotidyl transferase activity of the plant host or this mono-uridylation is performed by a viral factor.

GFLV RNA 3' terminal uridylation is restored *in vivo*

The design of GFLV infectious transcripts predates our discovery of GFLV RNA pervasive mono-uridylation. As a result, the infectious transcripts produced *in vitro* were not intentionally uridylated. For instance, the *in vitro* transcribed RNA1 and RNA2 that together form the synthetic GT isolate were designed to end by UAU(A)^{30}GC and UAU(A)^{22}G, respectively (Supplemental Data Set S2b) (Vigne et al., 2013). Because non-templated nucleotides are frequently added by T7 RNA polymerase during *in vitro* transcription, it cannot be excluded that some of these transcripts could end with a poly(A) tail and a uridine. However, such transcripts should be a minority in any case. Yet, the 3'RACE-seq analysis shown in Figure 8A using the GT isolate revealed that the vast majority of both RNA1 and RNA2 are mono-uridylated. This indicates that both GT RNA1 and RNA2's termini have been optimized when the GT isolate was multiplied *in planta*.

We independently verified this observation by using another synthetic isolate called K30. The *in vitro* transcribed RNA1 and RNA2 of the synthetic K30 isolate end by AUUUU(A)$_{31}$ and UUUAU(A)$_{22}$G, respectively (Supplemental Data Set S2b) (Vigne et al., 2013). We analyzed by 3'RACE-seq GFLV RNAs from plants infected by virions that were originally produced from quinoa plants infected with K30 infectious transcripts and propagated multiple times. As a control, we also analyzed plants infected with the B844 isolate which originates from infected grapevine and was also propagated multiple times in quinoa plants. 3'RACE-seq analysis revealed similar levels of RNA1 and RNA2 mono-uridylation for the K30 and B844 isolates (Figure 9). This result confirms that the extremities of non-uridylated *in vitro*-produced GFLV RNA1 and RNA2 were optimized *in planta* to restore the mono-uridylation of wild-type GFLV RNA poly(A) tails. This *in vivo* optimization strongly supports a pro-viral role of mono-uridylation of GFLV poly(A) tails, although we do not yet know its molecular function (see Discussion).

Finally, we investigated the genomic RNA1 and RNA2 uridylation level for the K30 and B844 isolates using purified virions. This analysis revealed that uridylation can reach up to 96.9% of the encapsidated GFLV RNAs (Figure 9). Therefore, mono-uridylation of poly(A) tails is a *bona fide* genomic feature of GFLV RNAs and corresponds to a hitherto unknown type of viral extremities. This genomic feature is shared by the two closely related nepoviruses GFLV and ArMV (Hily et al., 2021; Sanfaçon, 2022). Both viruses are the major causal agents of grapevine fanleaf degeneration disease, a yet incurable disease causing massive yield losses in the wine industry worldwide (Fuchs and Lemaire, 2017; Mannini and Digiaro, 2017; Schmitt-Keichinger et al., 2017).

Discussion

We report here that the 3' terminal uridylation patterns of phytoviral RNAs are extremely varied across single-stranded positive RNA phytoviruses. This diversity in the positions, composition and length of U- and U rich-tails indicates a hitherto unsuspected complexity of uridylation in phytoviral RNA metabolism. Because the uridylation sites reported here are detected in the 3' most terminal region of viral RNAs, additional upstream uridylation sites possibly exist and are yet to be explored. Other types of viral RNAs from negative strand or double stranded RNA viruses and transcripts from DNA viruses will also need to be analyzed to reveal the full complexity of uridylation patterns for phytoviruses.

We chose to use 3'RACE-seq which allows the analysis of 3' nucleotide extensions including the detection of at least one non-templated nucleotide added at 3' extremities. Our experimental approach is fundamentally different from the oligo(dA)-primed cDNA strategy used previously to investigate viral RNA uridylation (Huo et al., 2016). Although both studies conclude that uridylation is detected on all viral RNAs investigated and that it occurs frequently on truncated viral RNAs, the results remain hardly comparable because short tails, which represent the vast majority of nucleotide extensions, were not analyzed in (Huo et al., 2016). For instance, by mapping all 3' extremities of the TCV RNA, we detected three clusters of uridylation, including a cluster (cluster III) in the 3' last 5 nucleotides. Rather than uridylation, U-rich tails with complex consensus motifs were proposed in this region (Huo et al., 2016), and we did not confirm this observation. Also, we did not detect highly heteropolymeric tails on TMV or CMV RNAs in any of the biological replicates that we analyzed. One of the key advantages of 3' RACE-seq is to allow the investigation of 3' terminal uridylation of viral RNA poly(A) tails, and this was crucial to detect the high frequency of mono-uridylation for GFLV and ArMV RNAs. Importantly, such a mono-uridylation of poly(A) tails may have a pro-, rather than anti-, viral function(s) for the nepoviruses GFLV and ArMV. This hypothesis is supported by the high uridylation rate of encapsidated GFLV RNAs and by the *in planta* optimization of non-uridylated infectious transcripts. We show that the mono-uridylation of GFLV RNAs is not mediated by the two host TUTases reported to facilitate RNA decay. The addition of a single uridine by the viral RNA polymerase after completion of the poly(A) synthesis (which we show is at least partly templated by an oligo(U) sequence) is among the possible scenarios that should be considered in priority. Indeed, the addition of untemplated nucleotides has been reported for several viral RNA polymerases from various viruses including picornaviruses, caliciviruses, flaviviruses, nodaviruses, alphaviruses, hepaciviruses,

vesiculoviruses, coronaviruses and bacteriophage ϕ6 (Smallwood and Moyer, 1993; Neufeld et al., 1994; Behrens et al., 1996; Arnold and Cameron, 1999; Ranjith-Kumar et al., 2001; Rohayem et al., 2006; Tomar et al., 2006; Fullerton et al., 2007; Poranen et al., 2008; Wang et al., 2013; Wu et al., 2014; Tvarogová et al., 2019). Thus, the GFLV RNA polymerase RNA dependent RdRp, $1E^{Pol}$, is among the candidate factors to test whether it could add a single uridine after synthesizing the poly(A) tail of the positive strands. Adding a single uridine might facilitate the release of the RNA polymerase, which would constitute a pro-viral role for uridylation.

Another area of investigation is to determine whether the high rate of GFLV RNA uridylation is regulated *in planta*, and by what process. Indeed, the data shown in Figure 4 confirmed the high uridylation rates of GFLV RNAs as compared to other viral RNAs, but an intermediate level of uridylation was observed for GFLV RNA1 and RNA2 especially in the third replicate of infected quinoa plants. We checked that this decrease in uridylation is not due to a lower RNA quality of this sample. This observation raises the interesting possibility that GFLV RNA uridylation levels might be modulated by a yet unidentified condition *in planta*. Identifying this condition could be key to understand the precise function of GFLV RNA uridylation.

One of the important results of our study is that uridylation is frequently detected on degradation intermediates, such as truncated or oligo-adenylated viral RNAs. In addition, the proportion of TCV RNA degradation intermediates versus full-length RNA increases in the absence of the TUTases. This observation is in line with uridylation stimulating the degradation of phytoviral RNA, or at least viral RNA fragments, as it does for coding and non-coding cellular RNAs, and as it was proposed for Orsay virus in *C. elegans* and influenza A virus mRNAs in human cells (Le Pen et al., 2018). Yet, several of our observations indicate that uridylation could play complex roles during viral RNA degradation in plants. Firstly, the size of uridylated oligo(A) tails is unexpectedly variable across polyadenylated viral RNAs. For instance, uridylated oligo(A) tails are larger for PVX RNA than for TuMV RNA, for which this reduction in size is particularly obvious (Figure 3). Such a variation in uridylated oligo(A) tail sizes was not previously reported for mRNAs in Arabidopsis, suggesting a more complex interplay between deadenylation and uridylation processes for viral RNAs than for mRNAs (Sement et al., 2013; Zuber et al., 2016; Scheer et al., 2021). One of the possible explanations is that the size of mRNA uridylated oligo(A) tails is likely mostly determined by the competition between poly(A) binding proteins (PABPs), the deadenylation machinery and TUTases. By contrast, oligo(A) or poly(A) tails of viral RNAs may be involved in distinct processes, like forming triple RNA helices to stabilize the 3' end of viral RNAs or binding PAPBP (Tsai et al., 1999; Tycowski et al., 2012; Olsthoorn et al., 2022). Resolving these different structures or complexes will likely imply different processes and factors that will generate distinct degradation intermediates. Secondly, our analysis demonstrates that both host TUTases, URT1 and HESO1, differentially uridylate viral RNAs. Indeed, we have identified distinct patterns of uridylation for URT1 and HESO1, both for TCV and TuMV RNAs. In the case of TuMV RNAs, URT1 and HESO1 seem to uridylate oligo(A) tails of different sizes and add a distinct number of Us. The respective size of the oligo(A) and the U-tails could influence what factors bind to the corresponding TuMV RNA, and therefore URT1- or HESO1-mediated uridylation could trigger different fates, or specify different degradation pathways. It is also possible that distinct degradation intermediates of

TCV RNA that are uridylated by URT1 or HESO1 are degraded by distinct factors. In fact, because URT1 and HESO1 add different lengths of U-extensions and likely connect distinct cellular factors, uridylation may favor viral RNA degradation via cooperative pathways that need to be further explored. Finally, we recently reported that URT1-mediated uridylation prevents the excessive deadenylation of Arabidopsis mRNAs, which otherwise favors spurious siRNA biogenesis from endogenous mRNAs (Scheer et al., 2021). Therefore, the uridylation of oligo-adenylated viral RNAs as observed for TuMV may play an analogous role: in a wild-type plant, preventing excessive deadenylation could assist TuMV RNA to escape detection by the silencing machinery. Of note, initial experiments did not reveal significant variations of viral accumulation upon infection by TuMV of *urt1-1*, *heso1-4* or *heso1-4 urt1-1* double mutant (Supplemental Figure S7) and it is likely that dissecting the potential pro- and anti-viral roles of RNA uridylation will require adequate genetic backgrounds to counteract the robustness conferred by redundant processes involved in host-virus interactions. Also, studying viral RNA uridylation at each step of the virus cycle appears essential to decipher all pro-and anti-viral roles of uridylation.

Materials and Methods

Plant growth conditions

The Arabidopsis (*Arabidopsis thaliana*) plants used in this work are of Columbia accession (Col-0). Arabidopsis AGIs analyzed in this study were AT2G45620 (*URT1*) and AT2G39740 (*HESO1*). Arabidopsis mutants analyzed in this study are T-DNA insertion lines: *urt1-1* (SALK_087647C) (Sement et al., 2013) and *heso1-4* (GK-369H06-017072). *heso1-4 urt1-1* was obtained by crossing and provided by P. Brodersen (University of Copenhagen, Denmark). For virus propagation, plants were grown on soil in a neon-lit growth chamber under controlled temperature (18 to 21°C) with 12 h photoperiod conditions. *Nicotiana benthamiana* (wild-type and the *35S::B2:*GFP line[46]), *Nicotiana clevelandii*, spinach (*Spinacia oleracea*), quinoa (*Chenopodium quinoa*) and rapeseed (*Brassica napus*) plants used for agroinfiltration or virus inoculation were grown on soil with a 16 h light / 8 h darkness photoperiod in a greenhouse (at 21/18 °C). Infected grapevines (*Vitis vinifera*) originated from vineyards or from the INRAE-collection that were grown in individual pots to obtain two shoots of 180 cm, under natural light conditions.

Oligonucleotides.

Oligonucleotides used in this study are listed in Supplemental Data Set S1.

Virus strain and propagation

Details about virus isolates/strains, inoculations, hosts and harvesting are listed in Supplemental Data Set S2. Briefly, PVX and TRV were inoculated using agrobacterium (*Agrobacterium tumefaciens*) culture of infectious clones, GFLV and TMV using virions, BBWV-1, CMV, and PCV using viral RNAs, and TYMV using an infectious plasmid. TCV, TuMV, SoMV, AlMV, TBSV, BNYVV, ArMV (quinoa), TRSV, SLRSV (quinoa), GFLV (B844 isolate on quinoa), CNDV, CLRV, CPMV and RpRSV were inoculated by sap from infected tissues. TuYV was inoculated on *B. napus* by aphid transmission

(Leiser et al., 1992). Grapevine rootstocks Kober 5BB were infected by GFLV (isolate B844) and ArMV by heterologous grafting and infected-vines were cultivated in a greenhouse. GRSPaV, GPGV, GRGV, GVB, TBRV, SLRSV, GLRaV-1, and GLRaV-2 originate from infected vineyards or infected grapevine collection.

Virus purification

Viral particles of GFLV K30 and B844 isolates (described in Supplemental Data Set S2b) were purified from quinoa by sucrose gradient as described in (Schellenberger et al., 2011).

RNA extraction from infected plants or purified viruses

Total RNA from infected leaves was extracted using Tri-Reagent (Molecular Research Center) or using the RNeasy plant Mini Kit (Qiagen) following the manufacturer's instructions, except that the RLC lysis buffer was complemented with 25 mM DTT for herbaceous tissues or with 25 mM DTT and 1% (w/v) PVP40 (final concentrations) for grapevine tissues. GFLV K30 and GFLV B844 genomic RNAs were extracted from purified virions using phenol-chloroform. RNA concentrations were measured by spectrophotometry (Thermo Fisher scientific, Nanodrop 2000). RNA quality was checked by loading 200-400 ng total RNA on a 1% agarose gel.

Preparation of 3' and 5' RACE-seq libraries

3' RACE-seq libraries were prepared from 1-5 µg of total RNA according to (Scheer et al., 2021). Oligonucleotides used for library preparation are provided in Supplemental Data Set S1a and the full procedure is detailed in Supplemental Methods.

To analyze the 5' end sequence of the GFLV minus or plus strand, we set up a 5' RACE-seq strategy which combines cDNA synthesis using the 5' RACE System for Rapid Amplification of cDNA End (Invitrogen™, v2.0) and Illumina sequencing (Supplemental Figure S6). Briefly, 5 µg of total RNA extracted from Arabidopsis plants infected by GFLV (isolate GT) were used to synthesize a GFLV specific cDNA following the manufacturer's instructions. Three rounds of PCR were then performed to amplify the 5' region using GoTaq® DNA Polymerase (Promega) and 1-2 µL cDNA, PCR1 or PCR2. PCR cycles were as follows: a step at 94°C for 1 min; 25, 20 or 5 cycles (for PCR1, PCR2 or PCR3, respectively) at 94°C for 30 s, 55-65°C for 30 s and 72°C for 40 s; a final step at 72°C for 40 s. All used primers are listed in Supplemental Data Set S1a. All PCR3 products were purified using one volume of magnetic beads (AMPure XP Reagent for PCR purification, Beckman Coulter). Libraries were paired-end sequenced with MiSeq (v3 chemistry) with 41x111 bp cycle settings.

Data processing for 3' and 5' RACE-seq.

Fastq files were analyzed by a homemade pipeline adapted from (Scheer et al., 2021) and composed of scripts using Python (v2.7), Biopython (v1.63)(Cock et al., 2009) and RegEX (v2.4) libraries. Most steps of data processing are common between 3' and 5' RACE-seq data analyses. Bioinformatic protocols are detailed in Supplementary Methods and are available in Github (https://github.com/hzuber67/RACEseq_virus)

Quantification of TuMV RNA accumulation by RT-qPCR

RNA was extracted as described above from TuMV infected Arabidopsis leaves 14 days after infection. Five micrograms of total RNA were DNase-treated for 30 min at 37°C with 5 U of DNase I (Thermofisher) and 1X DNase I buffer (Thermofisher) in a final volume of 50 µL. DNase-treated RNA was purified by phenol-chloroform extraction and ethanol precipitation. cDNA synthesis was performed in a 20 µl reaction volume that contains 1 µg of purified DNase-treated RNA, 50 pmol of oligo$(dT)_{18}$ (Thermofisher), 50 ng of random hexamers (Thermofisher), 10 nmol of dNTPs, 0.1 µmol of DTT, 40 U of RNaseOUT (Invitrogen), 200 U of SuperScript IV reverse transcriptase (Invitrogen), and 1X of SuperScript IV RT buffer (Invitrogen). Reactions were incubated at 50 °C for 10 min, and then at 80 °C for 10 min to inactivate the reverse transcriptase. RT-qPCR was then performed using primers specific for the TuMV RNA or of the housekeeping gene *ACTIN2* of Arabidopsis (AT3G18780) (see primer sequences in Supplemental Data Set S1c). RT-qPCR was performed in a LightCycler® 480 II (Roche) in a 10 µl reaction volume containing 0.1 µL of cDNA, 2.5 µM of forward and reverse primers and 1X of SYBR green (Applied Biosystems). PCR cycles were as follows: a 5 min step of denaturation at 95°C, followed by 45 cycles of 10 s denaturation at 95 °C, 15 s annealing at 58 °C, 15 s elongation at 72 °C, and a final denaturation step of 5 s at 95 °C and a final elongation step of 1 min at 55°C. Cycle threshold (Ct) values were exported using the LightCycler 480 Software, (v 1.5.1). For each sample and primer pair, RT-qPCR reactions were performed in triplicates and triplicate CT values were averaged. TuMV RNA accumulation was finally calculated as a relative quantity normalized to *ACTIN2* RNA accumulation using the following formula: $2^{-(Ct^{TuMV} - Ct^{Actin2})}$. RT-qPCR analyses were performed for two biological replicates, *i.e.* two batches of eight to nine plants grown independently, for WT, *urt1-1*, heso1-4, and *heso1-4 urt1-1* Arabidopsis plants. Boxplot analysis shown in Supplemental Figure S7 displays the relative quantity of TuMV RNA for each biological replicate and genotype and colored points show the relative quantity for each individual plant.

Phylogenetic analysis

The phylogenetic tree in Supplemental Figure S2 show relationships among species of the Secoviridae family. The tree was calculated from the aligned amino acid sequences of the conserved protease-polymerase (Pro-Pol) region, from the protease CG motif to the polymerase GDD motif. Evolutionary analyses were conducted in MEGA X (Kumar et al. 2018). Alignments were performed using the MUSCLE program with default parameters. The evolutionary history was inferred by using the Maximum Likelihood method with the best fit model (LG) including a discrete Gamma distribution to model evolutionary rate differences among sites (5 categories, +*G* parameter = 3.53). The rate variation model allowed for some sites to be evolutionarily invariable ([+*I*], 0.05% sites). 1000 bootstrap replicates were performed. The tree was drawn to scale with branch lengths indicating the number of substitutions per site. The analyzed Secoviridae species and sequence accession numbers are as follows: GFLV (GQ332372, NC_003615, MF804979, JN391442, KC900162), ArMV (MW380904, BK059316, CQ369527, MN5999884, MH802018), RpRSV (MN384981, MZ220963, MZ291909, MW057710, AY310444), TRSV (MT210150, MT563078, MN504762, U50869, KJ556849),

TBRV (MW961144, MZ291911, MW057704, KX977560, MT992604), CLRV (NC_015414, KC937021, GU167974, LT883167, KU215412), CPMV (X00206, MT682297, MT815984, MT723988), BBWV1 (MN216348, AY781171, MF770979, AB084450, MZ202340), CNDV (MW848523, NC_038320, MW080951) and SLRSV (MF797011, MF796997, MF797001, NC-006964, MF796999).

Statistics and reproducibility

All plots were generated using R (v. 3.6.1) and the R package ggplot2 (v. 3.3.5) on RStudio (v. 1.4.1106). To compare uridylation percentages of viral RNAs (Figure 6A and Figure 7A), RNA fragment percentages (Figure 6F) and the frequency of each nucleotide before tail (Figure 6E) across genotypes, we used the R package car (v3.0-5) applying a generalized linear model for proportions with a quasibinomial distribution. To test the difference of U-tail sizes between genotype (Figure 7B), tail size medians were calculated for each infected plant and genotype and a non-parametric test was applied using Pairwise Wilcoxon Rank Sum Tests with data considered as unpaired (two-tailed). For Figure 3, Figure 7C and Supplemental Figure S7, a linear regression (R package stats, v3.6.1) was applied as visual examination of the QQ plots did not show evidence of non-normality. To test the difference of poly(A) tail sizes between uridylated and non-uridylated RNAs (Figure 3 and Figure 7C), poly(A) tail size medians were calculated for each individual plant and viral RNA, and pairwise comparisons were performed between uridylated and non-uridylated RNAs. The multcomp R package (1.4-19) with Tukey contrasts was used for multiple comparison post hoc tests and the calculation of adjusted p-values. For all statistical analyses, a p-value of 0.05 is defined as the threshold of significance. The number of independent biological replicates is indicated in each figure legend. Detailed results of the statistical analysis are provided in Supplemental Data Set S4 and S5.

Accession numbers

NGS datasets generated during this study have been deposited in NCBI's Gene Expression Omnibus (Edgar et al., 2002) and are accessible through the GEO Series accession number GSE212358 (https://www.ncbi.nlm.nih.gov/geo/query/acc.cgi?acc=GSE212358). GEO Series accession numbers for individual datasets are GSE212292 (for Figure 1, Figure 2, Figure 3 and Figure 5A, and Supplemental Figure 1, Supplemental Figure 3 and Supplemental Figure 4A), GSE212354 (for Figure 4), GSE212293 (for Figure 6, Figure 7 and Figure 8A, and Supplemental Figure 4A and Supplemental Figure 5), GSE212355 (for Figure 8B and Supplemental Figure S6B), and GSE212356 (for Figure 9). Source data for all figures are included as Supplemental Data Sets.

Bioinformatic pipelines including python and bash source code for 3'RACE-seq are available in Github (https://github.com/hzuber67/RACEseq_virus).

Funding

This work was supported by Centre National de la Recherche Scientifique (CNRS), Institut national de recherche pour l'agriculture, l'alimentation et l'environnement (INRAE), Université de Strasbourg and by a research grant from the French National Research Agency ANR-20-CE20-0010. Some of the sequencing experiments were supported by a funding from the state managed by the French National Research Agency as part of the "Investments for the Future" program under the framework of the LABEX: ANR-10-LABX-0036_NETRNA and ANR-17-EURE-0023.

Acknowledgments

The authors gratefully acknowledge Salah Bouzoubaah, Véronique Brault, Marc Fuchs, David Gilmer, Anthony Gobert, Manfred Heinlein, Jean-Sébastien Reynard, Christophe Ritzenthaler, Corinne Schmitt-Keichinger, Claire Villeroy and Véronique Ziegler-Graff for providing viruses or infected plant material analyzed in this study. The authors also thank Peter Brodersen for providing the *heso1-4 urt1-1* line, Anthony Gobert for sharing the experimental procedure for ligation of structured RNA and expressed their gratitude to David Gilmer, Heike Lange and Corinne Schmitt-Keichinger for helpful discussions. We also acknowledge the respective plant facility staff at IBMP and the experimental unit of INRAE Grand Est-Colmar for plant maintenance.

Author Contributions

ACJ and SG performed most of the experiments; HZ designed all bioinformatic analyses that were conducted by HZ and ACJ; HZ and ACJ produced all figures and associated datasets, except for the phylogenetic analysis of *Secoviridae* viruses performed by JMH; ACJ, SG, JMH, DGar, EV, GD, OL, HZ and DGag discussed and analyzed data; SK performed the MiSeq runs; HZ and DGag supervised the project; DGag initiated the project and acquired funding; HZ and DGag contributed equally to this work.

672

673 Conflict of interest statement. None declared.

674

675

676

Tables

Table 1: Representative species of single-stranded positive RNA phytoviruses analyzed in this study. The classification is according to ICTV Master Species List 2021.v1. Note that the nature of GLRaV-2 and CNDV 3' ends were reassessed in this study (see Figure 1). The gRNA column indicates the number of genomic RNA for each virus. VPg: viral protein genome-linked, TLS: tRNA-like structure.

Order	Family	Subfamily	Genus	Species	Acronym	gRNA	5' feature	3' end
Martellivirales	*Bromoviridae*	-	*Cucumovirus*	*Cucumber mosaic virus*	CMV	3	Cap	No polyA, TLS
		-	*Alfamovirus*	*Alfalfa mosaic virus*	AlMV	3	Cap	No polyA
	Closteroviridae	-	*Ampelovirus*	*Grapevine leafroll-associated virus 1*	GLRaV-1	1	Putative cap	No polyA
		-	*Closterovirus*	*Grapevine leafroll-associated virus 2*	GLRaV-2	1	Putative cap	A-rich
	Virgaviridae	-	*Pecluvirus*	*Peanut clump virus*	PCV	2	Cap	No polyA, TLS
		-	*Tobamovirus*	*Tobacco mosaic virus*	TMV	1	Cap	No polyA, TLS
		-	*Tobravirus*	*Tobacco rattle virus*	TRV	2	Cap	No polyA
Sobelivirales	*Solemoviridae*	-	*Polerovirus*	*Turnip yellows virus*	TuYV	1	VPg	No polyA
		-	*Sobemovirus*	*Sowbane mosaic virus*	SoMV	1	VPg	No polyA
Tolivirales	*Tombusviridae*	-	*Betacarmovirus*	*Turnip crinkle virus*	TCV	1	-	No polyA
		-	*Tombusvirus*	*Tomato bushy stunt virus*	TBSV	1	-	No polyA
Picornavirales	*Secoviridae*	*Comovirinae*	*Nepovirus*	*Grapevine fanleaf virus*	GFLV	2	VPg	polyA
		-	*Sequivirus*	*Carrot necrotic dieback virus*	CNDV	1	VPg	No polyA
Patatavirales	*Potyviridae*	-	*Potyvirus*	*Turnip mosaic virus*	TuMV	1	VPg	polyA
Hepelivirales	*Benyviridae*	-	*Benyvirus*	*Beet necrotic yellow vein virus*	BNYVV	4	Cap	polyA
Tymovirales	*Alphaflexviridae*	-	*Potexvirus*	*Potato virus X*	PVX	1	Cap	polyA
	Betaflexviridae	*Quinvirinae*	*Foveavirus*	*Grapevine rupestris stem pitting-associated virus*	GRSPaV	1	Putative cap	polyA
		Trivirinae	*Trichovirus*	*Grapevine Pinot gris virus*	GPGV	1	-	polyA
		Trivirinae	*Vitivirus*	*Grapevine virus B*	GVB	1	Putative cap	polyA
	Tymoviridae	-	*Maculavirus*	*Grapevine redglobe virus*	GRGV	1	Cap	polyA
		-	*Tymovirus*	*Turnip yellow mosaic virus*	TYMV	1	Cap	No polyA, TLS

684 **Table 2: Representative species of *Secoviridae* analyzed in this study.** The classification is according to ICTV Master Species List 2021.v1. Note that the
685 nature of CNDV 3' ends was reassessed in this study (see Figure 1). VPg: viral protein genome-linked. The gRNA column indicates the number of genomic
686 RNA for each virus.
687

Order	Family	Subfamily	Genus	Species	Acronym	gRNA	5' feature	3' end
Picornavirales	*Secoviridae*	*Comovirinae*	*Comovirus*	*Cowpea mosaic virus*	CPMV	2	VPg	polyA
			Fabavirus	*Broad bean wilt virus 1*	BBWV-1	2	VPg	polyA
			Nepovirus	*Raspberry ringspot virus*	RpRSV	2	VPg	polyA
				Tobacco ringspot virus	TRSV	2	VPg	polyA
				Grapevine fanleaf virus	GFLV	2	VPg	polyA
				Arabis mosaic virus	ArMV	2	VPg	polyA
				Tomato black ring virus	TBRV	2	VPg	polyA
				Cherry leaf roll virus	CLRV	2	VPg	polyA
		-	*Stralarivirus*	*Strawberry latent ringspot virus*	SLRSV	2	VPg	polyA
		-	*Sequivirus*	*Carrot necrotic dieback virus*	CNDV	1	VPg	No polyA

688

Figure legends

Figure 1: 3' terminal features of CNDV and GLRaV-2 RNAs. A, C, High-resolution mapping of 3' ends for CNDV (A) and GLRaV-2 (C) RNA. Heatmaps show frequencies of reads mapped to the indicated position for three infected plants. Position 0 corresponds to the 3' end of the full-length viral RNA. B, D, Percentage of tailed vs non-tailed reads found at the last 3' end position for CNDV (B) and GLRaV-2 (D) RNAs. E, Examples of A-rich tails added to GLRaV-2 RNA. F, Sequence logo generated from GLRaV-2 RNA tails containing G. 42 to 66% of all tails (i.e. regardless of their internal or 3' terminal position) contain G. Plant hosts and virus isolates are indicated in Supplemental Data Set S2.

Figure 2: U-tailing of ss(+) RNA phytoviruses is widespread and diverse. A, Uridylation percentages of phytoviral RNAs. Each bar represents an infected plant (n=2 for GVB and n=3 for all other viruses). The percentages of long (> 1 nt) and 1 nt U-tails are indicated by dark gray and light gray, respectively. B, Proportion of the different U-tail sizes from 1 to 30 nt. Percentages were calculated using the number of U-tailed reads as denominator. U-tail sizes are indicated by a color gradient from light purple, for 1U, to black for 20 to 30 Us. Only viral RNAs for which uridylation was detected for at least 50 reads per replicate are shown. TLS in red indicates viral RNAs ending with a tRNA-like sequence. Plant hosts are indicated in Supplemental Data Set S2A.

Figure 3: Boxplot analysis comparing the size of non-modified poly(A) tails vs uridylated poly(A) tails for polyadenylated viral RNAs. Each boxplot represents an infected plant (n=3) and displays the median, first and third quartiles (lower and upper hinges), the largest value within 1.5 times the interquartile range above the upper hinge (upper whisker) and the smallest value within 1.5 times the interquartile range below the lower hinge (lower whiskers). Only viral RNAs for which uridylation was detected for at least 50 reads per replicate are shown. Plant hosts are indicated in Supplemental Data Set S2a. Stars represent significant statistical p-value (linear model, F-statistic, n=3) with $p < 0.01$ (**) or 0.001 (***).

Figure 4: High uridylation levels are restricted to GFLV and ArMV. A, Uridylation percentages among the *Secoviridae* family. Each bar represents an infected plant, the host plant is indicated below and virus isolates are indicated in Supplemental Data Set S2b. The percentages of long (> 1 nt) and 1 nt U-tails are indicated by dark gray and light gray, respectively. Percentages shown for GFLV in *Vitis spp.* and CNDV were calculated from the same dataset used in Figure 2. No data were obtained for the BBWV-1 RNA2 for unknown technical reasons. The diagram (not to scale) below barplots illustrates the phylogenetic distances between the *Secoviridae* viruses analyzed in this study. The phylogenetic tree is shown in Supplemental Figure S2. B, Proportion of the different U-tail sizes from 1 to 30 nt. The percentages were calculated using the number of U-tails as denominator. U tail sizes are indicated by a color gradient from light purple for 1-nt U-tails to black for 20 to 30-nt U-tails. Only viral RNAs for which uridylation was detected for at least 50 reads per replicate are shown.

Figure 5: Uridylation of degradation intermediates reveals patterns of ribonucleolytic attacks. A, High-resolution mapping of RNA 3' ends for a selection of non-polyadenylated viral RNAs (indicated on the left). Frequencies of reads at each 3' end position are shown by a blue color scale for non-tailed reads and an orange color scale for U-tailed reads. Frequencies were calculated using the total number of reads as denominator. Position 0 corresponds to the 3' end of the full-length viral RNA. For each virus, three infected plants were analyzed. B, Secondary structure and tertiary interactions in the 3′ UTR of TCV RNA according to (McCormack et al., 2008; Simon, 2015). The TCV 3' UTR contains one weak (M3H) and five stable hairpins (H4, H4a, H4b, H5 and Pr) as well as three H-type pseudoknots (Y1, Y2, Y3) shown as red arrows. The frequency of uridylated 3' ends detected in infected *N. benthamiana* plants is indicated by colored rectangles for each uridylation site. The three detected clusters of uridylation sites are highlighted in yellow. Plant hosts are indicated in Supplemental Data Set S2A.

Figure 6: Contribution of the Arabidopsis TUTases in the uridylation of TCV RNAs. A, Uridylation percentages of TCV RNA in infected WT, *urt1-1*, *heso1-4* and *heso1-4 urt1-1* plants. Percentages are shown for tails containing only Us (U-tail, left panel) or a majority of Us (U-rich, right panel). Each bar represents an individual plant (n=3). The percentages of long (> 1 nt) and 1 nt U-tails are indicated by dark gray and light gray, respectively. Significantly different values ($p < 0.05$) are labelled by different letters (generalized linear model for proportion, quasibinomial distribution). B-D, High resolution mapping of TCV RNA 3' ends in infected WT, *urt1-1*, *heso1-4* and *heso1-4 urt1-1* plants. A close-up view is shown for the three detected clusters of uridylation. Frequencies were calculated using the total number of reads as denominator. Frequencies of non-tailed, U-tailed and U-rich-tailed reads at each 3' end position are shown by blue, orange and green color scales, respectively. Position 0 corresponds to the 3' end of full-length TCV RNA. E, Relative frequency, compared to WT, of the last nucleotide before U-tails and U-rich tails in *urt1-1* and *heso1-4* mutants. Stars represent significant statistical p-value (generalized linear model for proportion, quasibinomial distribution, n=3) with $p < 0.001$. F, Proportion of TCV RNA degradation intermediates in infected WT, *urt1-1*, *heso1-4* and *heso1-4 urt1-1* plants. Each bar represents an individual plant (n=3). The percentages of full-length RNAs, with 3' end located in a 5 nt window upstream the 3' end, and of RNA fragments are indicated by dark gray and light gray, respectively. Significantly different values ($p < 0.05$) are labelled by different letters (generalized linear model for proportion, quasibinomial distribution).

Figure 7: Both URT1 and HESO1 contribute to the uridylation of TuMV RNA. A, Percentages of uridylation of TuMV RNA in infected WT, *urt1-1*, *heso1-4* and *heso1-4 urt1-1* Arabidopsis plants. Each bar represents an infected plant (n=6). Percentages of long (> 1 nt) and 1 nt U-tails are indicated by dark gray and light gray, respectively. Significantly different values ($p<0.05$) are labelled by different letters (generalized linear model for proportion, quasibinomial distribution). B, Proportion of the different U-tail sizes from 1 to 30 nt. Percentages were calculated using the number of U-tailed reads as denominator. Individual points are color-coded for each of the six replicates. U-tail size medians are

indicated by red arrows. Significantly different medians of U-tail sizes ($p<0.05$) are labelled by different letters (two-tailed Wilcoxon rank-sum test, n=6). C, Boxplot analysis comparing non-modified poly(A) tails (turquoise) vs uridylated poly(A) tails (gray). Each boxplot represents an infected plant (n=6) and displays the median, first and third quartiles (lower and upper hinges), the largest value within 1.5 times the interquartile range above the upper hinge (upper whisker) and the smallest value within 1.5 times the interquartile range below the lower hinge (lower whiskers). Boxplots for *heso1-4 urt1-1* plants are not shown as uridylation is almost abrogated. Stars represent significant statistical p-value (linear model, F-statistic, n=3) with $p < 0.001$ (***). D, Distribution of poly(A) tail sizes of non-tailed (turquoise) or uridylated (gray) viral RNAs for WT, *urt1-1*, *heso1-4* and *heso1-4 urt1-1* plants infected by TuMV. Percentages were calculated using the total number of sequences with tails from 1 to 89 nucleotides as denominator. Individual points are color-coded for each of the six replicates. The gray area indicates the average of all replicates.

Figure 8: Arabidopsis TUTases are not required to maintain uridylation of GFLV RNAs. A, Uridylation percentages of GFLV RNAs (isolate GT) in infected WT, *urt1-1*, *heso1-4* and *heso1-4 urt1-1* Arabidopsis plants. Each bar represents an infected plant (n=8). The percentages of long (> 1 nt) and 1 nt U-tails are indicated by dark gray and light gray, respectively. Of note, almost all GFLV RNAs (from 99.72 to 100%) end with a single U. B, 5' and 3' features of GFLV RNA 1 and RNA2 negative strands. Upper part: Diagram illustrating the 3' and 5' extremities of the GFLV RNA plus and minus strands deduced from 3' and 5' RACE-seq results. The GFLV isolate GT was used. Lower part: Percentages of nucleotide additions at the 5' (right) and 3' (left) end of the minus strands. Proportions of the different tail sizes are shown for U-tails detected at the 5' end of the minus strand. The percentages were calculated using the number of U-tails as denominator. U-tail sizes are indicated by a red gradient from light red, for 1-nt U-tails, to dark red, for 31-nt U-tails and longer. Each bar represents an infected plant (n=3 for 5' end and n=4 for 3' end).

Figure 9: Uridylation is a genomic feature of encapsidated GFLV RNAs. Uridylation frequencies of GFLV RNAs (K30 and B844 isolates) for total RNA of *C. quinoa* infected plants or for encapsidated RNAs. For each of the two GFLV isolates, one replicate was analyzed. The percentages of long (> 1 nt) and 1 nt U-tails are indicated by dark gray and light gray, respectively. Of note, almost all GFLV RNAs (from 99.76 to 99.92%) end with a single U.

References

Arnold JJ, Cameron CE (1999) Poliovirus RNA-dependent RNA polymerase (3Dpol) is sufficient for template switching in vitro. Journal of Biological Chemistry **274**: 2706–2716

Behrens SE, Tomei L, De Francesco R (1996) Identification and properties of the RNA-dependent RNA polymerase of hepatitis C virus. EMBO J **15**: 12–22

Calil IP, Fontes EPB (2017) Plant immunity against viruses: antiviral immune receptors in focus. Ann Bot **119**: 711–723

Cock PJA, Antao T, Chang JT, Chapman BA, Cox CJ, Dalke A, Friedberg I, Hamelryck T, Kauff F, Wilczynski B, et al. (2009) Biopython: freely available Python tools for computational molecular biology and bioinformatics. Bioinformatics **25**: 1422–1423

De Almeida C, Scheer H, Zuber H, Gagliardi D (2018) RNA uridylation: a key post-transcriptional modification shaping the coding and non-coding transcriptome. WIREs RNA e1440

Dreher TW (2010) Viral tRNAs and tRNA-like structures. Wiley Interdiscip Rev RNA **1**: 402–414

Edgar R, Domrachev M, Lash AE (2002) Gene Expression Omnibus: NCBI gene expression and hybridization array data repository. Nucleic Acids Res **30**: 207–210

Faehnle CR, Walleshauser J, Joshua-Tor L (2014) Mechanism of Dis3l2 substrate recognition in the Lin28-let-7 pathway. Nature **514**: 252–256

Fuchs M, Lemaire O (2017) Novel Approaches for Viral Disease Management. *In* B Meng, GP Martelli, DA Golino, M Fuchs, eds, Grapevine Viruses: Molecular Biology, Diagnostics and Management. Springer International Publishing, Cham, pp 599–621

Fullerton SWB, Blaschke M, Coutard B, Gebhardt J, Gorbalenya A, Canard B, Tucker PA, Rohayem J (2007) Structural and functional characterization of sapovirus RNA-dependent RNA polymerase. J Virol **81**: 1858–1871

Hily JM, Poulicard N, Kubina J, Reynard JS, Spilmont AS, Fuchs M, Lemaire O, Vigne E (2021) Metagenomic analysis of nepoviruses: diversity, evolution and identification of a genome region in members of subgroup A that appears to be important for host range. Arch Virol **166**: 2789–2801

Hulo C, de Castro E, Masson P, Bougueleret L, Bairoch A, Xenarios I, Le Mercier P (2011) ViralZone: a knowledge resource to understand virus diversity. Nucleic Acids Res **39**: D576-582

Huo Y, Shen J, Wu H, Zhang C, Guo L, Yang J, Li W (2016) Widespread 3′-end uridylation in eukaryotic RNA viruses. Sci Rep **6**: 25454

Kumar S, Stecher G, Li M, Knyaz C, Tamura K (2018) MEGA X: Molecular Evolutionary Genetics Analysis across Computing Platforms. Mol Biol Evol **35**:1547–1549

Le M-T, Kasprzak WK, Kim T, Gao F, Young MY, Yuan X, Shapiro BA, Seog J, Simon AE (2017) Folding behavior of a T-shaped, ribosome-binding translation enhancer implicated in a wide-spread conformational switch. eLife **6**: e22883

Le Pen J, Jiang H, Di Domenico T, Kneuss E, Kosałka J, Leung C, Morgan M, Much C, Rudolph KLM, Enright AJ, et al. (2018) Terminal uridylyltransferases target RNA viruses as part of the innate immune system. Nat Struct Mol Biol **25**: 778–786

Leiser RM, Ziegler-Graff V, Reutenauer A, Herrbach E, Lemaire O, Guilley H, Richards K, Jonard G (1992) Agroinfection as an alternative to insects for infecting plants with beet western yellows luteovirus. Proc Natl Acad Sci U S A **89**: 9136–9140

Liu Y-P, Peremyslov VV, Medina V, Dolja VV (2009) Tandem leader proteases of Grapevine leafroll-associated virus-2: Host-specific functions in the infection cycle. Virology **383**: 291–299

Malecki M, Viegas SC, Carneiro T, Golik P, Dressaire C, Ferreira MG, Arraiano CM (2013) The exoribonuclease Dis3L2 defines a novel eukaryotic RNA degradation pathway. EMBO J **32**: 1842–1854

Mannini F, Digiaro M (2017) The effects of viruses and viral diseases on grapes and wine. *In* B Meng, GP Martelli, DA Golino, M Fuchs, eds, Grapevine Viruses: Molecular Biology, Diagnostics and Management. Springer International Publishing, Cham, pp 453–482

Martin IR, Vigne E, Velt A, Hily J-M, Garcia S, Baltenweck R, Komar V, Rustenholz C, Hugueney P, Lemaire O, et al. (2021) Severe stunting symptoms upon Nepovirus infection are reminiscent of a chronic hypersensitive-like response in a perennial woody fruit crop. Viruses **13**: 2138

McCormack JC, Yuan X, Yingling YG, Kasprzak W, Zamora RE, Shapiro BA, Simon AE (2008) Structural domains within the 3' untranslated region of Turnip crinkle virus. J Virol **82**: 8706–8720

Menzel W, Vetten HJ (2008) Complete nucleotide sequence of an isolate of the Anthriscus strain of Parsnip yellow fleck virus. Arch Virol **153**: 2173–2175

Morozov IY, Jones MG, Gould PD, Crome V, Wilson JB, Hall AJW, Rigden DJ, Caddick MX (2012) mRNA 3' tagging is induced by nonsense-mediated decay and promotes ribosome dissociation. Mol Cell Biol **32**: 2585–2595

Neufeld KL, Galarza JM, Richards OC, Summers DF, Ehrenfeld E (1994) Identification of terminal adenylyl transferase activity of the poliovirus polymerase 3Dpol. J Virol **68**: 5811–5818

Olsthoorn RC, Mertens S, Brederode FT, Bol JF (1999) A conformational switch at the 3' end of a plant virus RNA regulates viral replication. EMBO J **18**: 4856–4864

Olsthoorn RCL, Owen CA, Livieratos IC (2022) Role of an RNA pseudoknot involving the polyA tail in replication of Pepino mosaic potexvirus and related plant viruses. Sci Rep **12**: 11532

Poranen MM, Koivunen MRL, Bamford DH (2008) Nontemplated terminal nucleotidyltransferase activity of double-stranded RNA bacteriophage phi6 RNA-dependent RNA polymerase. J Virol **82**: 9254–9264

Ranjith-Kumar CT, Gajewski J, Gutshall L, Maley D, Sarisky RT, Kao CC (2001) Terminal nucleotidyl transferase activity

of recombinant Flaviviridae RNA-dependent RNA polymerases: implication for viral RNA synthesis. J Virol **75**: 8615–8623
Ren G, Chen X, Yu B (2012) Uridylation of miRNAs by hen1 suppressor1 in Arabidopsis. Curr Biol **22**: 695–700
Ritzenthaler C, Viry M, Pinck M, Margis R, Fuchs M, Pinck LY 1991 (1991) Complete nucleotide sequence and genetic organization of grapevine fanleaf nepovirus RNA1. Journal of General Virology **72**: 2357–2365
Rohayem J, Jäger K, Robel I, Scheffler U, Temme A, Rudolph W (2006) Characterization of norovirus 3Dpol RNA-dependent RNA polymerase activity and initiation of RNA synthesis. J Gen Virol **87**: 2621–2630
Sanfaçon H (2022) Re-examination of nepovirus polyprotein cleavage sites highlights the diverse specificities and evolutionary relationships of nepovirus 3C-like proteases. Arch Virol **167**: 2529–2543
Scheer H, de Almeida C, Ferrier E, Simonnot Q, Poirier L, Pflieger D, Sement FM, Koechler S, Piermaria C, Krawczyk P, et al (2021) The TUTase URT1 connects decapping activators and prevents the accumulation of excessively deadenylated mRNAs to avoid siRNA biogenesis. Nat Commun **12**: 1298
Scheer H, De Almeida C, Sikorska N, Koechler S, Gagliardi D, Zuber H (2020) High-Resolution Mapping of 3' Extremities of RNA Exosome Substrates by 3' RACE-Seq. Methods Mol Biol **2062**: 147–167
Scheer H, Zuber H, De Almeida C, Gagliardi D (2016) Uridylation earmarks mRNAs for degradation… and more. Trends in Genetics **32**: 607–619
Schellenberger P, Demangeat G, Lemaire O, Ritzenthaler C, Bergdoll M, Oliéric V, Sauter C, Lorber B (2011) Strategies for the crystallization of viruses : using phase diagrams and gels to produce 3D crystals of Grapevine fanleaf virus. J Struct Biol **174**: 344–351
Schmitt-Keichinger C, Hemmer C, Berthold F, Ritzenthaler C (2017) Molecular, cellular, and structural biology of grapevine fanleaf virus. *In* B Meng, GP Martelli, DA Golino, M Fuchs, eds, Grapevine Viruses: Molecular Biology, Diagnostics and Management. Springer International Publishing, Cham, pp 83–107
Sement FM, Ferrier E, Zuber H, Merret R, Alioua M, Deragon J-M, Bousquet-Antonelli C, Lange H, Gagliardi D (2013) Uridylation prevents 3' trimming of oligoadenylated mRNAs. Nucleic Acids Res **41**: 7115–7127
Serghini MA, Fuchs M, Pinck M, Reinbolt J, Walter B, Pinck L (1990) RNA2 of grapevine fanleaf virus : sequence analysis and coat protein cistron location. J Gen Virol **71**: 1433–1441
Simon AE (2015) 3'UTRs of carmoviruses. Virus Res **206**: 27–36
Smallwood S, Moyer SA (1993) Promoter analysis of the vesicular stomatitis virus RNA polymerase. Virology **192**: 254–263
Tomar S, Hardy RW, Smith JL, Kuhn RJ (2006) Catalytic core of alphavirus nonstructural protein nsP4 possesses terminal adenylyltransferase activity. J Virol **80**: 9962–9969
Tsai CH, Cheng CP, Peng CW, Lin BY, Lin NS, Hsu YH (1999) Sufficient length of a poly(A) tail for the formation of a potential pseudoknot is required for efficient replication of bamboo mosaic potexvirus RNA. J Virol **73**: 2703–2709
Tu B, Liu L, Xu C, Zhai J, Li S, Lopez MA, Zhao Y, Yu Y, Ramachandran V, Ren G, et al. (2015) Distinct and cooperative activities of HESO1 and URT1 nucleotidyl transferases in microRNA turnover in Arabidopsis. PLoS Genet **11**: e1005119
Tvarogová J, Madhugiri R, Bylapudi G, Ferguson LJ, Karl N, Ziebuhr J (2019) Identification and characterization of a human coronavirus 229E nonstructural protein 8-associated RNA 3'-terminal adenylyltransferase activity. J Virol **93**: e00291-19
Tycowski KT, Shu M-D, Borah S, Shi M, Steitz JA (2012) Conservation of a Triple-Helix-Forming RNA Stability Element in Noncoding and Genomic RNAs of Diverse Viruses. Cell Reports **2**: 26–32
Vigne E, Gottula J, Schmitt-Keichinger C, Komar V, Ackerer L, Belval L, Rakotomalala L, Lemaire O, Ritzenthaler C, Fuchs M (2013) A strain-specific segment of the RNA-dependent RNA polymerase of grapevine fanleaf virus determines symptoms in Nicotiana species. J Gen Virol **94**: 2803–2813
Wang Z, Qiu Y, Liu Y, Qi N, Si J, Xia X, Wu D, Hu Y, Zhou X (2013) Characterization of a nodavirus replicase revealed a de novo initiation mechanism of RNA synthesis and terminal nucleotidyltransferase activity. J Biol Chem **288**: 30785–30801
Warkocki Z, Liudkovska V, Gewartowska O, Mroczek S, Dziembowski A (2018) Terminal nucleotidyl transferases (TENTs) in mammalian RNA metabolism. Philos Trans R Soc Lond, B, Biol Sci **373**: 20180162
Wu W, Wang Z, Xia H, Liu Y, Qiu Y, Liu Y, Hu Y, Zhou X (2014) Flock house virus RNA polymerase initiates RNA synthesis de novo and possesses a terminal nucleotidyl transferase activity. PLoS One **9**: e86876
Yu S, Kim VN (2020) A tale of non-canonical tails: gene regulation by post-transcriptional RNA tailing. Nat Rev Mol Cell Biol **21**: 542–556
Yuan X, Shi K, Simon AE (2012) A local, interactive network of 3' RNA elements supports translation and replication of Turnip crinkle virus. J Virol **86**: 4065–4081
Zhang W, Murphy C, Sieburth LE (2010) Conserved RNaseII domain protein functions in cytoplasmic mRNA decay and suppresses Arabidopsis decapping mutant phenotypes. Proc Natl Acad Sci USA **107**: 15981–15985
Zhao Y, Yu Y, Zhai J, Ramachandran V, Dinh TT, Meyers BC, Mo B, Chen X (2012) The Arabidopsis nucleotidyl transferase HESO1 uridylates unmethylated small RNAs to trigger their degradation. Curr Biol **22**: 689–694
Zhu HY, Ling KS, Goszczynski DE, McFerson JR, Gonsalves D (1998) Nucleotide sequence and genome organization of grapevine leafroll-associated virus-2 are similar to beet yellows virus, the closterovirus type member. J Gen Virol **79 (Pt 5)**: 1289–1298
Zigáčková D, Vaňáčová Š (2018) The role of 3' end uridylation in RNA metabolism and cellular physiology. Philos Trans R Soc Lond, B, Biol Sci **373**: 20180171
Zuber H, Scheer H, Ferrier E, Sement FM, Mercier P, Stupfler B, Gagliardi D (2016) Uridylation and PABP cooperate to repair mRNA deadenylated ends in Arabidopsis. Cell Rep **14**: 2707–2717
Zuber H, Scheer H, Joly A-C, Gagliardi D (2018) Respective contributions of URT1 and HESO1 to the uridylation of 5′

927 fragments produced from RISC-cleaved mRNAs. Front Plant Sci **9**: 1438
928

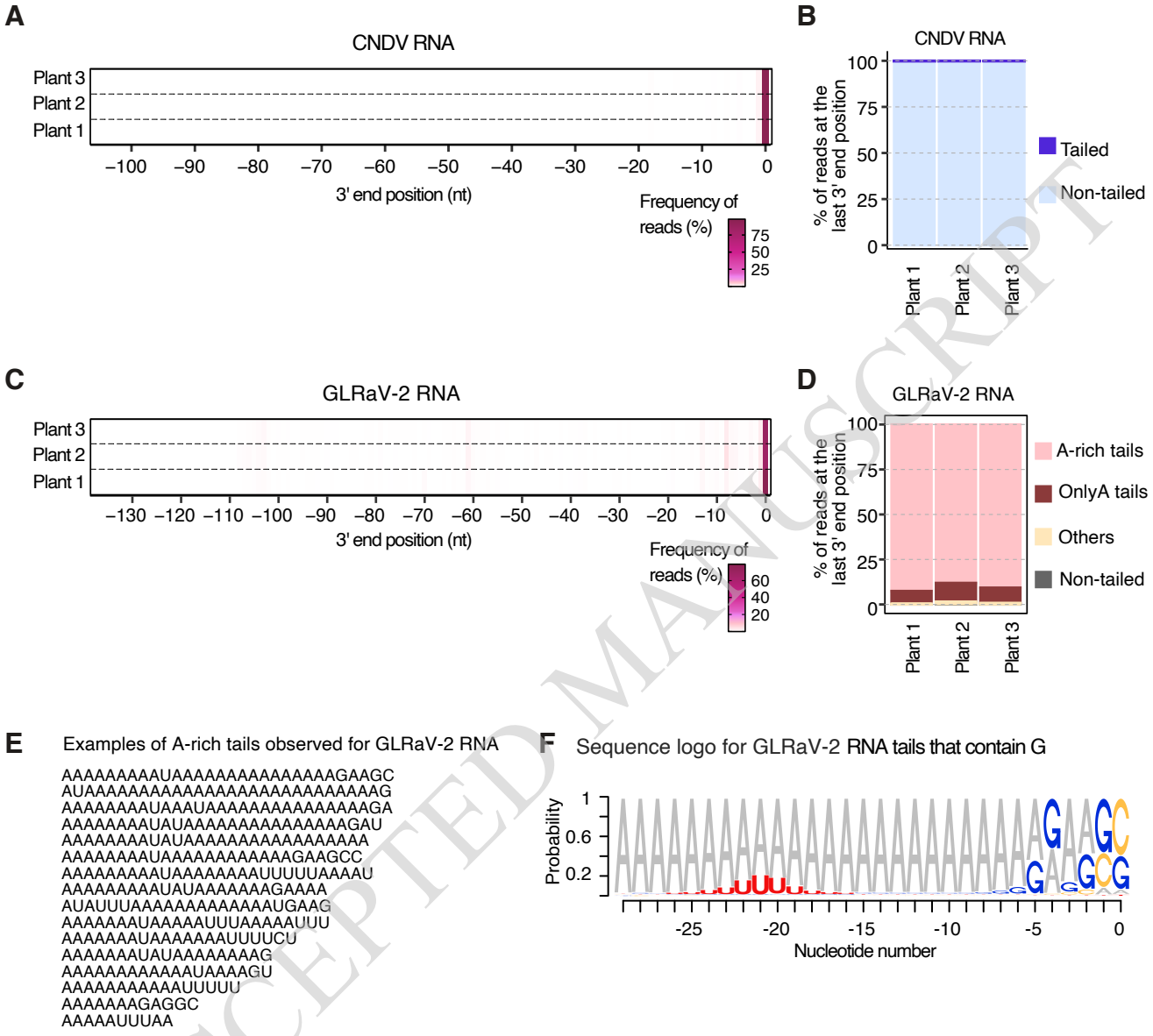

Figure 1: 3' terminal features of CNDV and GLRaV-2 RNAs. A, C, High-resolution mapping of 3' ends for CNDV (A) and GLRaV-2 (C) RNA. Heatmaps show frequencies of reads mapped to the indicated position for three infected plants. Position 0 corresponds to the 3' end of the full-length viral RNA. B, D, Percentage of tailed vs non-tailed reads found at the last 3' end position for CNDV (B) and GLRaV-2 (D) RNAs. E, Examples of A-rich tails added to GLRaV-2 RNA. F, Sequence logo generated from GLRaV-2 RNA tails containing G. 42 to 66% of all tails (i.e. regardless of their internal or 3' terminal position) contain G. Plant hosts and virus isolates are indicated in Supplemental Data Set S2.

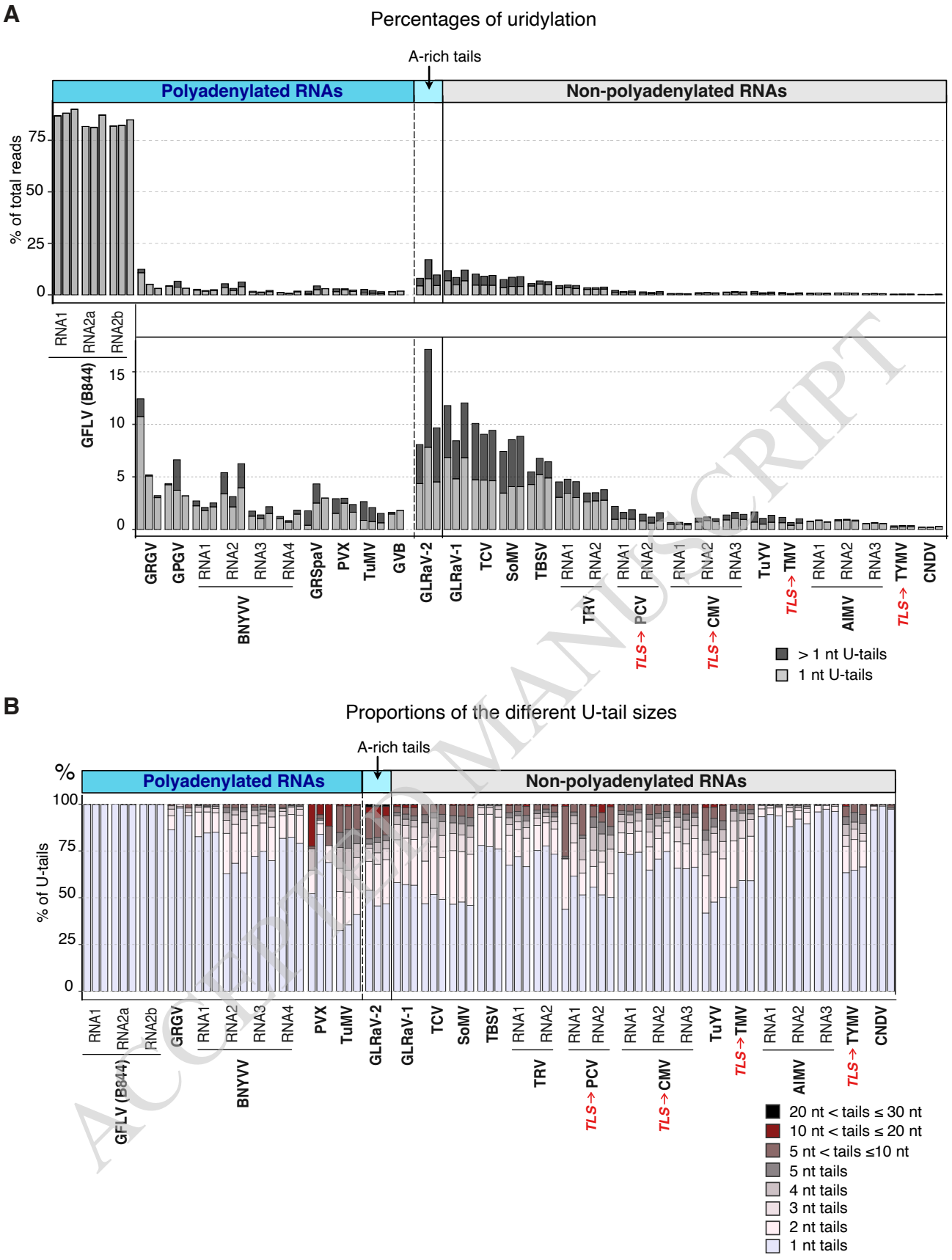

Figure 2: U-tailing of ss(+) RNA phytoviruses is widespread and diverse. A, Uridylation percentages of phytoviral RNAs. Each bar represents an infected plant (n=2 for GVB and n=3 for all other viruses). The percentages of long (> 1 U) and 1 U-tails are indicated by dark gray and light gray, respectively. B, Proportion of the different U-tail sizes from 1 to 30 nt. Percentages were calculated using the number of U-tailed reads as denominator. U-tail sizes are indicated by a color gradient from light purple, for 1U, to black for 20 to 30 Us. Only viral RNAs for which uridylation was detected for at least 50 reads per replicate are shown. TLS in red indicates viral RNAs ending with a tRNA-like sequence. Plant hosts are indicated in Supplemental Data Set S2A.

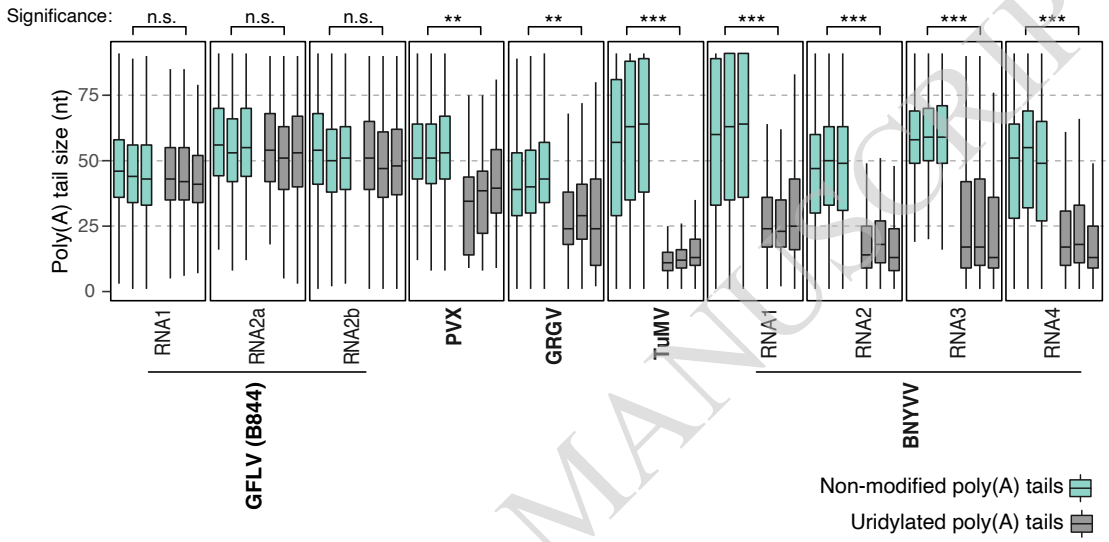

Figure 3: Boxplot analysis comparing the size of non-modified poly(A) tails vs uridylated poly(A) tails for polyadenylated viral RNAs. Each boxplot represents an infected plant (n=3) and displays the median, first and third quartiles (lower and upper hinges), the largest value within 1.5 times the interquartile range above the upper hinge (upper whisker) and the smallest value within 1.5 times the interquartile range below the lower hinge (lower whiskers). Only viral RNAs for which uridylation was detected for at least 50 reads per replicate are shown. Plant hosts are indicated in Supplemental Table 2a. Stars represent significant statistical p-value (linear model, n=3) with $p < 0.01$ (**) or 0.001 (***).

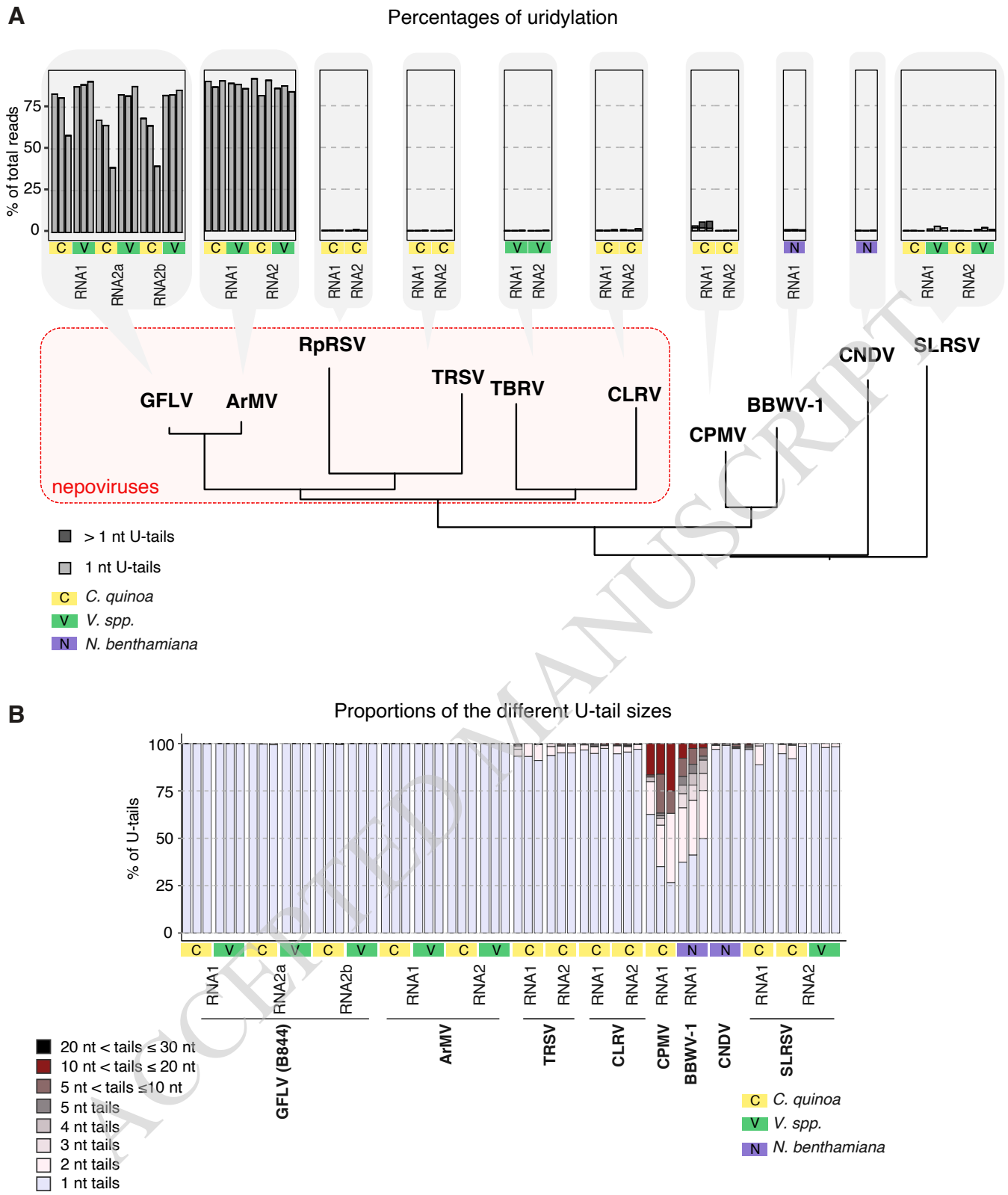

Figure 4: High uridylation levels are restricted to GFLV and ArMV. A, Uridylation percentages among the *Secoviridae* family. Each bar represents an infected plant, the host plant is indicated below and virus isolates are indicated in Supplemental Data Set S2b. The percentages of long (> 1 U) and 1 U-tails are indicated by dark gray and light gray, respectively. Percentages shown for GFLV in *Vitis spp.* and CNDV were calculated from the same dataset used in Figure 2. No data were obtained for the BBWV-1 RNA2 for unknown technical reasons. The diagram below barplots illustrates the phylogenetic distances between the *Secoviridae* viruses analyzed in this study. The phylogenetic tree is shown in Supplemental Figure S6B. B, Proportion of the different U-tail sizes from 1 to 30 nt. The percentages were calculated using the number of U-tails as denominator. U tail sizes are indicated by a color gradient from light purple for 1-nt U-tails to black for 20 to 30-nt U-tails. Only viral RNAs for which uridylation was detected for at least 50 reads per replicate are shown.

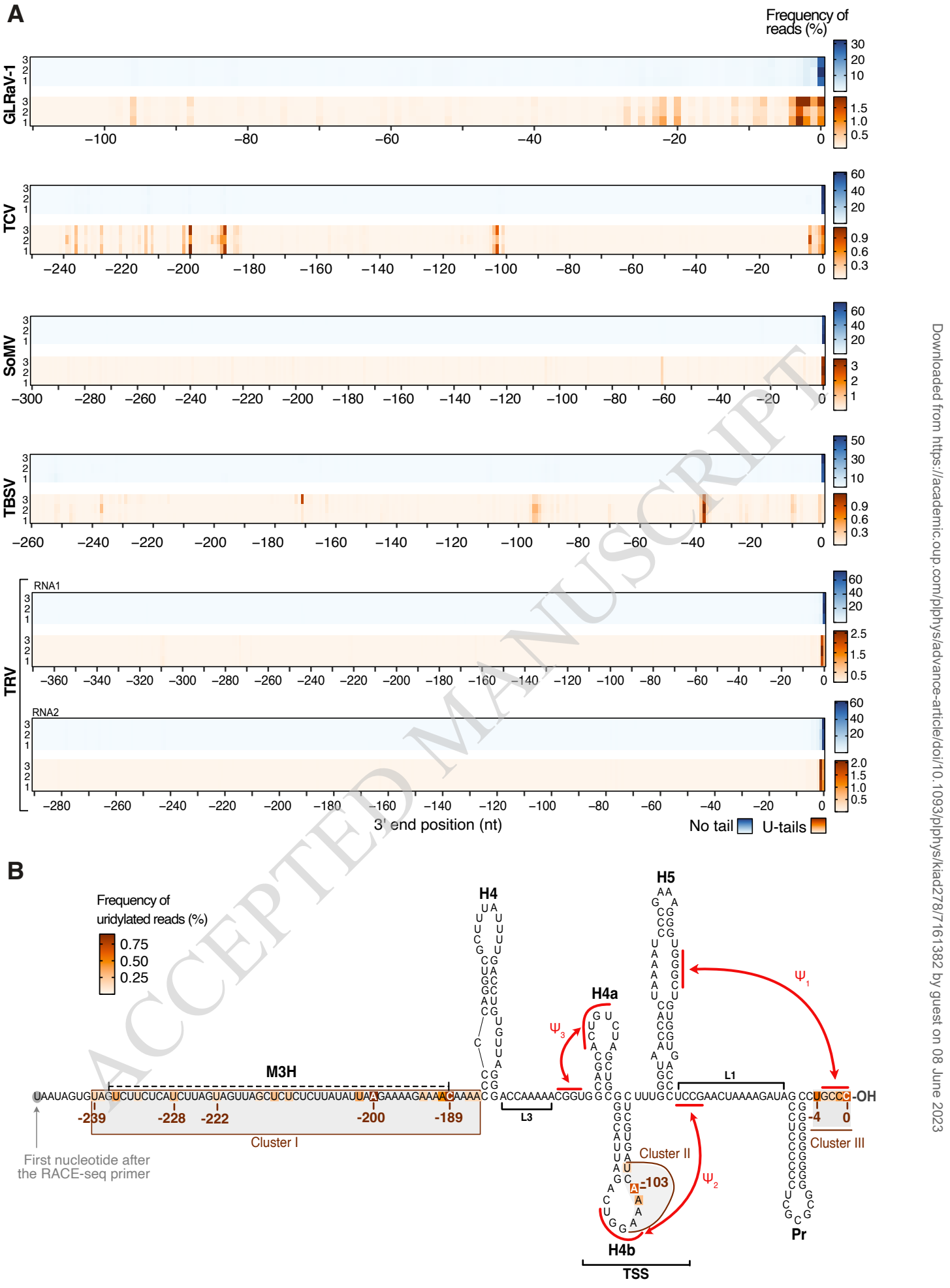

Figure 5: Uridylation of degradation intermediates reveals patterns of ribonucleolytic attacks. A, High-resolution mapping of RNA 3' ends for a selection of non-polyadenylated viral RNAs (indicated on the left). Frequencies of reads at each 3' end position are shown by a blue color scale for non-tailed reads and an orange color scale for U-tailed reads. Frequencies were calculated using the total number of reads as denominator. Position 0 corresponds to the 3' end of the full-length viral RNA. For each virus, three infected plants were analyzed. B, Secondary structure and tertiary interactions in the 3′ UTR of TCV RNA according to (McCormack et al., 2008; Simon, 2015). The TCV 3' UTR contains one weak (M3H) and five stable hairpins (H4, H4a, H4b, H5 and Pr) as well as three H-type pseudoknots (Y1, Y2, Y3) shown as red arrows. The frequency of uridylated 3' ends detected in infected *N. benthamiana* plants is indicated by colored rectangles for each uridylation site. The three detected clusters of uridylation sites are highlighted in yellow. Plant hosts are indicated in Supplemental Data Set S2a.

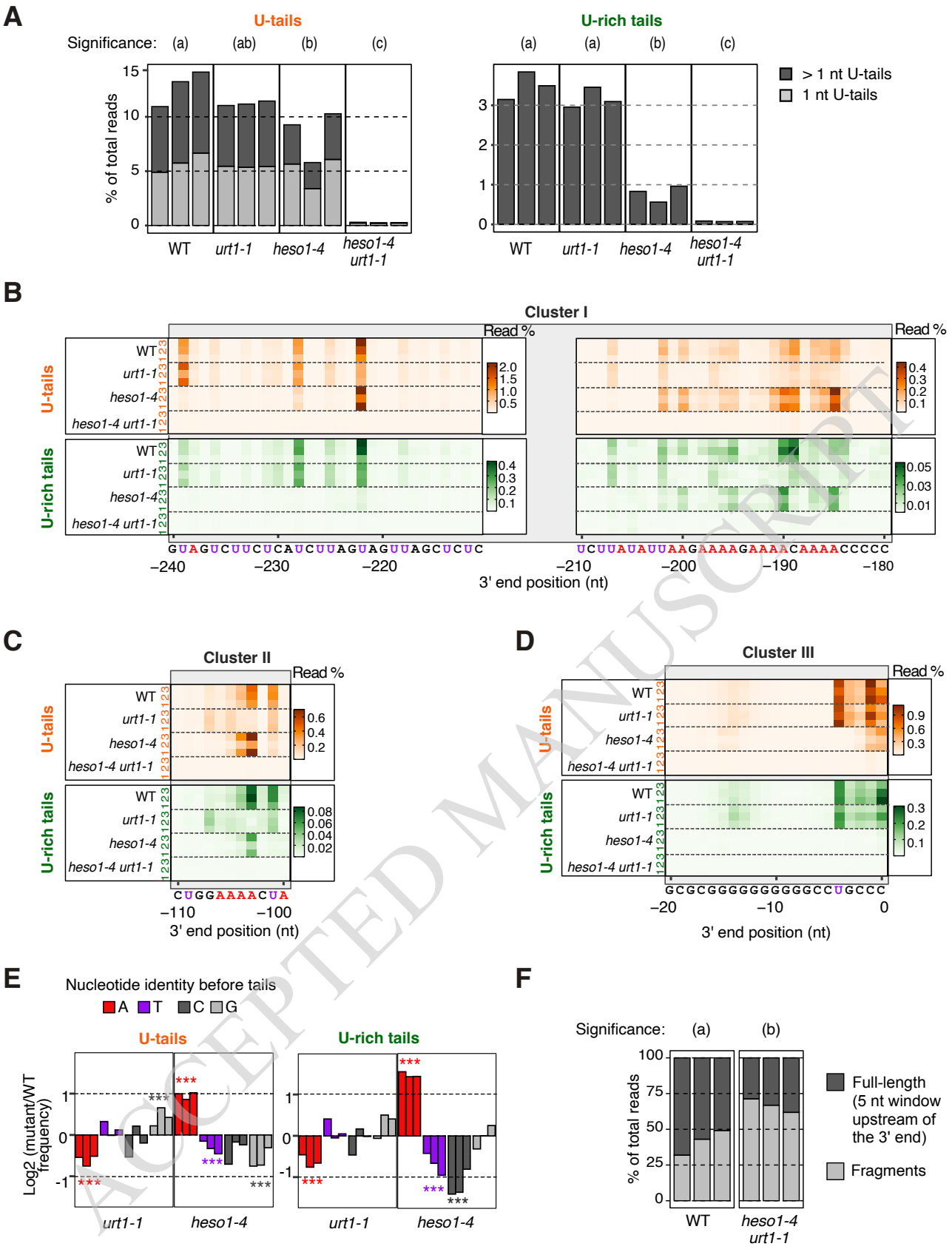

Figure 6: Contribution of the Arabidopsis TUTases in the uridylation of TCV RNAs. A, Uridylation percentages of TCV RNA in infected WT, *urt1-1*, *heso1-4* and *heso1-4 urt1-1* plants. Percentages are shown for tails containing only Us (U-tail, left panel) or a majority of Us (U-rich, right panel). Each bar represents an individual plant (n=3). The percentages of long (> 1 U) and 1 U-tails are indicated by dark gray and light gray, respectively. Significantly different values ($p < 0.05$) are labelled by different letters (generalized linear model for proportion, quasibinomial distribution. B-D, High resolution mapping of TCV RNA 3' ends in infected WT, *urt1-1*, *heso1-4* and *heso1-4 urt1-1* plants. A close-up view is shown for the three detected clusters of uridylation. Frequencies were calculated using the total number of reads as denominator. Frequencies of non-tailed, U-tailed and U-rich-tailed reads at each 3' end position are shown by blue, orange and green color scales, respectively. Position 0 corresponds to the 3' end of full-length TCV RNA. E, Relative frequency, compared to WT, of the last nucleotide before U-tails and U-rich tails in urt1-1 and heso1-4 mutants. Stars represent significant statistical p-value (generalized linear model for proportion, quasibinomial distribution, n=3) with $p < 0.001$. F, Proportion of TCV RNA degradation intermediates in infected WT, *urt1-1*, *heso1-4* and *heso1-4 urt1-1* plants. Each bar represents an individual plant (n=3). The percentages of full-length RNAs, with 3' end located in a 5 nt window upstream the 3' end, and of RNA fragments are indicated by dark gray and light gray, respectively. Significantly different values ($p < 0.05$) are labelled by different letters (generalized linear model for proportion, quasibinomial distribution).

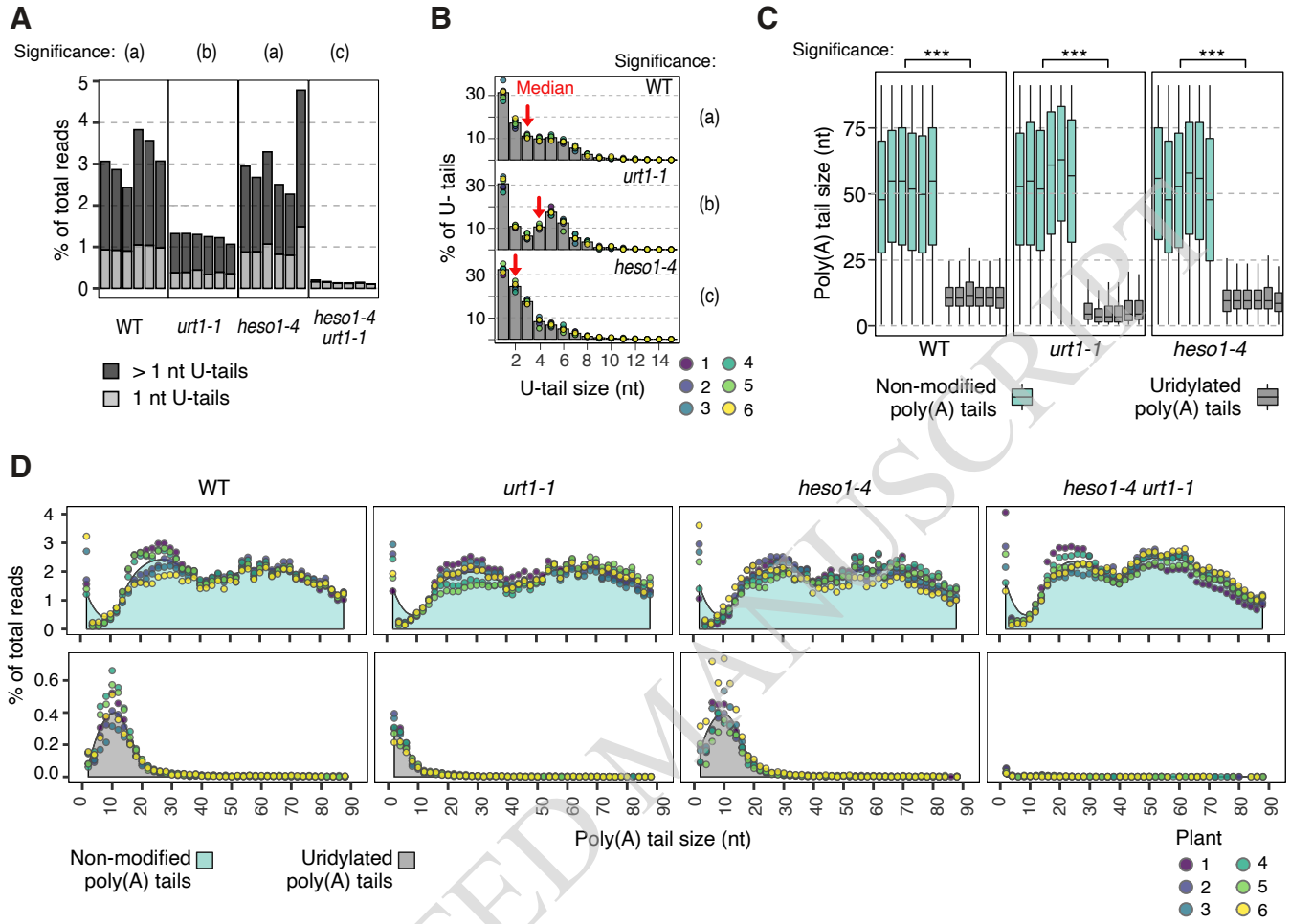

Figure 7: Both URT1 and HESO1 contribute to the uridylation of TuMV RNA. A, Percentages of uridylation of TuMV RNA in infected WT, *urt1-1*, *heso1-4* and *heso1-4 urt1-1* Arabidopsis plants. Each bar represents an infected plant (n=6). Percentages of long (> 1 U) and 1 U-tails are indicated by dark gray and light gray, respectively. Significantly different values ($p<0.05$) are labelled by different letters (generalized linear model for proportion, quasibinomial distribution). B, Proportion of the different U-tail sizes from 1 to 30 nt. Percentages were calculated using the number of U-tailed reads as denominator. Individual points are color-coded for each of the six replicates. U-tail size medians are indicated by red arrows. Significantly different medians of U-tail sizes ($p<0.05$) are labelled by different letters (two-tailed Wilcoxon rank-sum test, n=6). C, Boxplot analysis comparing non-modified poly(A) tails (turquoise) vs uridylated poly(A) tails (gray). Each boxplot represents an infected plant (n=6) and displays the median, first and third quartiles (lower and upper hinges), the largest value within 1.5 times the interquartile range above the upper hinge (upper whisker) and the smallest value within 1.5 times the interquartile range below the lower hinge (lower whiskers). Boxplots *for heso1-4 urt1-1* plants are not shown as uridylation is almost abrogated. Stars represent significant statistical p-value (linear model, n=3) with $p < 0.001$ (***). D, Distribution of poly(A) tail sizes of non-tailed (turquoise) or uridylated (gray) viral RNAs for WT, *urt1-1*, *heso1-4* and *heso1-4 urt1-1* plants infected by TuMV. Percentages were calculated using the total number of sequences with tails from 1 to 89 nucleotides as denominator. Individual points are color-coded for each of the six replicates. The gray area indicates the average of all replicates.

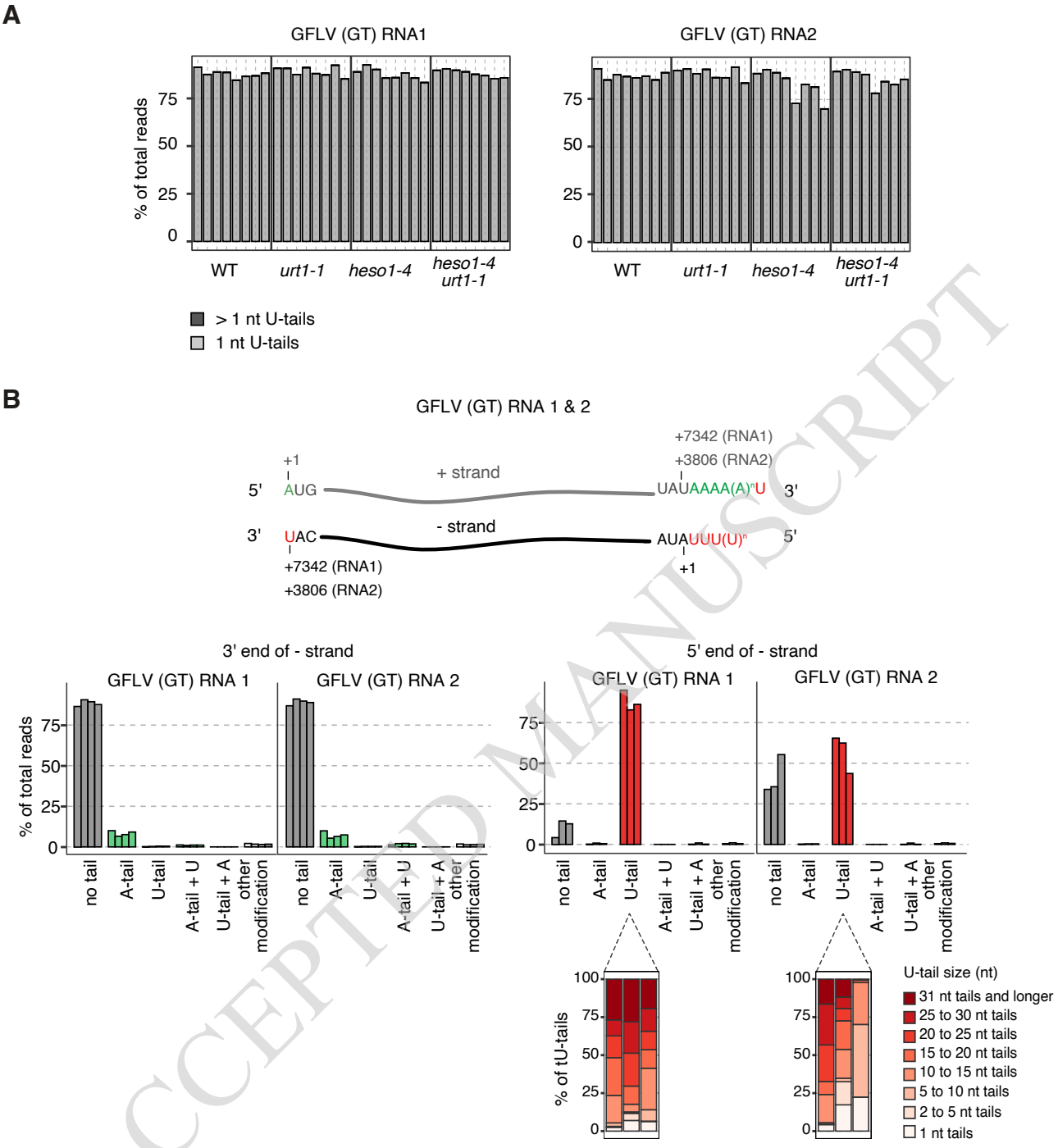

Figure 8: Arabidopsis TUTases are not required to maintain uridylation of GFLV RNAs. A, Uridylation percentages of GFLV RNAs (isolate GT) in infected WT, *urt1-1*, *heso1-4* and *heso1-4 urt1-1* Arabidopsis plants. Each bar represents an infected plant (n=8). The percentages of long (> 1 U) and 1 U-tails are indicated by dark gray and light gray, respectively. Of note, almost all GFLV RNAs (from 99.72 to 100%) end with a single U. B, 5' and 3' features of GFLV RNA 1 and RNA2 negative strands. Upper part: Diagram illustrating the 3' and 5' extremities of the GFLV RNA plus and minus strands deduced from 3' and 5' RACE-seq results. The GFLV isolate GT was used. Lower part: Percentages of nucleotide additions at the 5' (right) and 3' (left) end of the minus stands. Proportions of the different tail sizes are shown for U-tails detected at the 5' end of the minus strand. The percentages were calculated using the number of U-tails as denominator. U-tail sizes are indicated by a red gradient from light red, for 1-nt U-tails, to dark red, for 31-nt U-tails and longer. Each bar represents an infected plant (n=3 for 5' end and n=4 for 3' end).

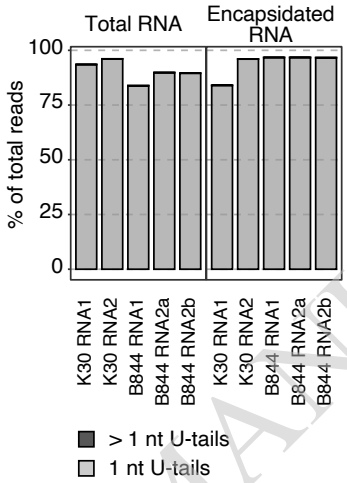

Figure 9: Uridylation is a genomic feature of encapsidated GFLV RNAs. Uridylation frequencies of GFLV RNAs (K30 and B844 isolates) for total RNA of *C. quinoa* infected plants or for encapsidated RNAs. For each of the two GFLV isolates, one replicate was analyzed. The percentages of long (> 1 U) and 1 U-tails are indicated by dark gray and light gray, respectively. Of note, almost all GFLV RNAs (from 99.76 to 99.92%) end with a single U.

Parsed Citations

Arnold JJ, Cameron CE (1999) Poliovirus RNA-dependent RNA polymerase (3Dpol) is sufficient for template switching in vitro. Journal of Biological Chemistry 274: 2706–2716
Google Scholar: Author Only Title Only Author and Title

Behrens SE, Tomei L, De Francesco R (1996) Identification and properties of the RNA-dependent RNA polymerase of hepatitis C virus. EMBO J 15: 12–22
Google Scholar: Author Only Title Only Author and Title

Calil IP, Fontes EPB (2017) Plant immunity against viruses: antiviral immune receptors in focus. Ann Bot 119: 711–723
Google Scholar: Author Only Title Only Author and Title

Cock PJA, Antao T, Chang JT, Chapman BA, Cox CJ, Dalke A, Friedberg I, Hamelryck T, Kauff F, Wilczynski B, et al. (2009) Biopython: freely available Python tools for computational molecular biology and bioinformatics. Bioinformatics 25: 1422–1423
Google Scholar: Author Only Title Only Author and Title

De Almeida C, Scheer H, Zuber H, Gagliardi D (2018) RNA uridylation: a key post-transcriptional modification shaping the coding and non-coding transcriptome. WIREs RNA e1440
Google Scholar: Author Only Title Only Author and Title

Dreher TW (2010) Viral tRNAs and tRNA-like structures. Wiley Interdiscip Rev RNA 1: 402–414
Google Scholar: Author Only Title Only Author and Title

Edgar R, Domrachev M, Lash AE (2002) Gene Expression Omnibus: NCBI gene expression and hybridization array data repository. Nucleic Acids Res 30: 207–210
Google Scholar: Author Only Title Only Author and Title

Faehnle CR, Walleshauser J, Joshua-Tor L (2014) Mechanism of Dis3l2 substrate recognition in the Lin28-let-7 pathway. Nature 514: 252–256
Google Scholar: Author Only Title Only Author and Title

Fuchs M, Lemaire O (2017) Novel Approaches for Viral Disease Management. In B Meng, GP Martelli, DA Golino, M Fuchs, eds, Grapevine Viruses: Molecular Biology, Diagnostics and Management. Springer International Publishing, Cham, pp 599–621
Google Scholar: Author Only Title Only Author and Title

Fullerton SWB, Blaschke M, Coutard B, Gebhardt J, Gorbalenya A, Canard B, Tucker PA, Rohayem J (2007) Structural and functional characterization of sapovirus RNA-dependent RNA polymerase. J Virol 81: 1858–1871
Google Scholar: Author Only Title Only Author and Title

Hily JM, Poulicard N, Kubina J, Reynard JS, Spilmont AS, Fuchs M, Lemaire O, Vigne E (2021) Metagenomic analysis of nepoviruses: diversity, evolution and identification of a genome region in members of subgroup A that appears to be important for host range. Arch Virol 166: 2789–2801
Google Scholar: Author Only Title Only Author and Title

Hulo C, de Castro E, Masson P, Bougueleret L, Bairoch A, Xenarios I, Le Mercier P (2011) ViralZone: a knowledge resource to understand virus diversity. Nucleic Acids Res 39: D576-582
Google Scholar: Author Only Title Only Author and Title

Huo Y, Shen J, Wu H, Zhang C, Guo L, Yang J, Li W (2016) Widespread 3′-end uridylation in eukaryotic RNA viruses. Sci Rep 6: 25454
Google Scholar: Author Only Title Only Author and Title

Kumar S, Stecher G, Li M, Knyaz C, Tamura K (2018) MEGA X: Molecular Evolutionary Genetics Analysis across Computing Platforms. Mol Biol Evol 35:1547–1549
Google Scholar: Author Only Title Only Author and Title

Le M-T, Kasprzak WK, Kim T, Gao F, Young MY, Yuan X, Shapiro BA, Seog J, Simon AE (2017) Folding behavior of a T-shaped, ribosome-binding translation enhancer implicated in a wide-spread conformational switch. eLife 6: e22883
Google Scholar: Author Only Title Only Author and Title

Le Pen J, Jiang H, Di Domenico T, Kneuss E, Kosałka J, Leung C, Morgan M, Much C, Rudolph KLM, Enright AJ, et al. (2018) Terminal uridylyltransferases target RNA viruses as part of the innate immune system. Nat Struct Mol Biol 25: 778–786
Google Scholar: Author Only Title Only Author and Title

Leiser RM, Ziegler-Graff V, Reutenauer A, Herrbach E, Lemaire O, Guilley H, Richards K, Jonard G (1992) Agroinfection as an alternative to insects for infecting plants with beet western yellows luteovirus. Proc Natl Acad Sci U S A 89: 9136–9140
Google Scholar: Author Only Title Only Author and Title

Liu Y-P, Peremyslov VV, Medina V, Dolja VV (2009) Tandem leader proteases of Grapevine leafroll-associated virus-2: Host-

specific functions in the infection cycle. Virology 383: 291–299
Google Scholar: Author Only Title Only Author and Title

Malecki M, Viegas SC, Carneiro T, Golik P, Dressaire C, Ferreira MG, Arraiano CM (2013) The exoribonuclease Dis3L2 defines a novel eukaryotic RNA degradation pathway. EMBO J 32: 1842–1854
Google Scholar: Author Only Title Only Author and Title

Mannini F, Digiaro M (2017) The effects of viruses and viral diseases on grapes and wine. In B Meng, GP Martelli, DA Golino, M Fuchs, eds, Grapevine Viruses: Molecular Biology, Diagnostics and Management. Springer International Publishing, Cham, pp 453–482
Google Scholar: Author Only Title Only Author and Title

Martin IR, Vigne E, Velt A, Hily J-M, Garcia S, Baltenweck R, Komar V, Rustenholz C, Hugueney P, Lemaire O, et al. (2021) Severe stunting symptoms upon Nepovirus infection are reminiscent of a chronic hypersensitive-like response in a perennial woody fruit crop. Viruses 13: 2138
Google Scholar: Author Only Title Only Author and Title

McCormack JC, Yuan X, Yingling YG, Kasprzak W, Zamora RE, Shapiro BA, Simon AE (2008) Structural domains within the 3' untranslated region of Turnip crinkle virus. J Virol 82: 8706–8720
Google Scholar: Author Only Title Only Author and Title

Menzel W, Vetten HJ (2008) Complete nucleotide sequence of an isolate of the Anthriscus strain of Parsnip yellow fleck virus. Arch Virol 153: 2173–2175
Google Scholar: Author Only Title Only Author and Title

Morozov IY, Jones MG, Gould PD, Crome V, Wilson JB, Hall AJW, Rigden DJ, Caddick MX (2012) mRNA 3' tagging is induced by nonsense-mediated decay and promotes ribosome dissociation. Mol Cell Biol 32: 2585–2595
Google Scholar: Author Only Title Only Author and Title

Neufeld KL, Galarza JM, Richards OC, Summers DF, Ehrenfeld E (1994) Identification of terminal adenylyl transferase activity of the poliovirus polymerase 3Dpol. J Virol 68: 5811–5818
Google Scholar: Author Only Title Only Author and Title

Olsthoorn RC, Mertens S, Brederode FT, Bol JF (1999) A conformational switch at the 3' end of a plant virus RNA regulates viral replication. EMBO J 18: 4856–4864
Google Scholar: Author Only Title Only Author and Title

Olsthoorn RCL, Owen CA, Livieratos IC (2022) Role of an RNA pseudoknot involving the polyA tail in replication of Pepino mosaic potexvirus and related plant viruses. Sci Rep 12: 11532
Google Scholar: Author Only Title Only Author and Title

Poranen MM, Koivunen MRL, Bamford DH (2008) Nontemplated terminal nucleotidyltransferase activity of double-stranded RNA bacteriophage phi6 RNA-dependent RNA polymerase. J Virol 82: 9254–9264
Google Scholar: Author Only Title Only Author and Title

Ranjith-Kumar CT, Gajewski J, Gutshall L, Maley D, Sarisky RT, Kao CC (2001) Terminal nucleotidyl transferase activity of recombinant Flaviviridae RNA-dependent RNA polymerases: implication for viral RNA synthesis. J Virol 75: 8615–8623
Google Scholar: Author Only Title Only Author and Title

Ren G, Chen X, Yu B (2012) Uridylation of miRNAs by hen1 suppressor1 in Arabidopsis. Curr Biol 22: 695–700
Google Scholar: Author Only Title Only Author and Title

Ritzenthaler C, Viry M, Pinck M, Margis R, Fuchs M, Pinck LY 1991 (1991) Complete nucleotide sequence and genetic organization of grapevine fanleaf nepovirus RNA1. Journal of General Virology 72: 2357–2365
Google Scholar: Author Only Title Only Author and Title

Rohayem J, Jäger K, Robel I, Scheffler U, Temme A, Rudolph W (2006) Characterization of norovirus 3Dpol RNA-dependent RNA polymerase activity and initiation of RNA synthesis. J Gen Virol 87: 2621–2630
Google Scholar: Author Only Title Only Author and Title

Sanfaçon H (2022) Re-examination of nepovirus polyprotein cleavage sites highlights the diverse specificities and evolutionary relationships of nepovirus 3C-like proteases. Arch Virol 167: 2529–2543
Google Scholar: Author Only Title Only Author and Title

Scheer H, de Almeida C, Ferrier E, Simonnot Q, Poirier L, Pflieger D, Sement FM, Koechler S, Piermaria C, Krawczyk P, et al (2021) The TUTase URT1 connects decapping activators and prevents the accumulation of excessively deadenylated mRNAs to avoid siRNA biogenesis. Nat Commun 12: 1298
Google Scholar: Author Only Title Only Author and Title

Scheer H, De Almeida C, Sikorska N, Koechler S, Gagliardi D, Zuber H (2020) High-Resolution Mapping of 3' Extremities of RNA

Exosome Substrates by 3' RACE-Seq. Methods Mol Biol 2062: 147–167
Google Scholar: Author Only Title Only Author and Title

Scheer H, Zuber H, De Almeida C, Gagliardi D (2016) Uridylation earmarks mRNAs for degradation... and more. Trends in Genetics 32: 607–619
Google Scholar: Author Only Title Only Author and Title

Schellenberger P, Demangeat G, Lemaire O, Ritzenthaler C, Bergdoll M, Oliéric V, Sauter C, Lorber B (2011) Strategies for the crystallization of viruses : using phase diagrams and gels to produce 3D crystals of Grapevine fanleaf virus. J Struct Biol 174: 344–351
Google Scholar: Author Only Title Only Author and Title

Schmitt-Keichinger C, Hemmer C, Berthold F, Ritzenthaler C (2017) Molecular, cellular, and structural biology of grapevine fanleaf virus. In B Meng, GP Martelli, DA Golino, M Fuchs, eds, Grapevine Viruses: Molecular Biology, Diagnostics and Management. Springer International Publishing, Cham, pp 83–107
Google Scholar: Author Only Title Only Author and Title

Sement FM, Ferrier E, Zuber H, Merret R, Alioua M, Deragon J-M, Bousquet-Antonelli C, Lange H, Gagliardi D (2013) Uridylation prevents 3' trimming of oligoadenylated mRNAs. Nucleic Acids Res 41: 7115–7127
Google Scholar: Author Only Title Only Author and Title

Serghini MA, Fuchs M, Pinck M, Reinbolt J, Walter B, Pinck L (1990) RNA2 of grapevine fanleaf virus : sequence analysis and coat protein cistron location. J Gen Virol 71: 1433–1441
Google Scholar: Author Only Title Only Author and Title

Simon AE (2015) 3'UTRs of carmoviruses. Virus Res 206: 27–36
Google Scholar: Author Only Title Only Author and Title

Smallwood S, Moyer SA (1993) Promoter analysis of the vesicular stomatitis virus RNA polymerase. Virology 192: 254–263
Google Scholar: Author Only Title Only Author and Title

Tomar S, Hardy RW, Smith JL, Kuhn RJ (2006) Catalytic core of alphavirus nonstructural protein nsP4 possesses terminal adenylyltransferase activity. J Virol 80: 9962–9969
Google Scholar: Author Only Title Only Author and Title

Tsai CH, Cheng CP, Peng CW, Lin BY, Lin NS, Hsu YH (1999) Sufficient length of a poly(A) tail for the formation of a potential pseudoknot is required for efficient replication of bamboo mosaic potexvirus RNA. J Virol 73: 2703–2709
Google Scholar: Author Only Title Only Author and Title

Tu B, Liu L, Xu C, Zhai J, Li S, Lopez MA, Zhao Y, Yu Y, Ramachandran V, Ren G, et al. (2015) Distinct and cooperative activities of HESO1 and URT1 nucleotidyl transferases in microRNA turnover in Arabidopsis. PLoS Genet 11: e1005119
Google Scholar: Author Only Title Only Author and Title

Tvarogová J, Madhugiri R, Bylapudi G, Ferguson LJ, Karl N, Ziebuhr J (2019) Identification and characterization of a human coronavirus 229E nonstructural protein 8-associated RNA 3'-terminal adenylyltransferase activity. J Virol 93: e00291-19
Google Scholar: Author Only Title Only Author and Title

Tycowski KT, Shu M-D, Borah S, Shi M, Steitz JA (2012) Conservation of a Triple-Helix-Forming RNA Stability Element in Noncoding and Genomic RNAs of Diverse Viruses. Cell Reports 2: 26–32
Google Scholar: Author Only Title Only Author and Title

Vigne E, Gottula J, Schmitt-Keichinger C, Komar V, Ackerer L, Belval L, Rakotomalala L, Lemaire O, Ritzenthaler C, Fuchs M (2013) A strain-specific segment of the RNA-dependent RNA polymerase of grapevine fanleaf virus determines symptoms in Nicotiana species. J Gen Virol 94: 2803–2813
Google Scholar: Author Only Title Only Author and Title

Wang Z, Qiu Y, Liu Y, Qi N, Si J, Xia X, Wu D, Hu Y, Zhou X (2013) Characterization of a nodavirus replicase revealed a de novo initiation mechanism of RNA synthesis and terminal nucleotidyltransferase activity. J Biol Chem 288: 30785–30801
Google Scholar: Author Only Title Only Author and Title

Warkocki Z, Liudkovska V, Gewartowska O, Mroczek S, Dziembowski A (2018) Terminal nucleotidyl transferases (TENTs) in mammalian RNA metabolism. Philos Trans R Soc Lond, B, Biol Sci 373: 20180162
Google Scholar: Author Only Title Only Author and Title

Wu W, Wang Z, Xia H, Liu Y, Qiu Y, Liu Y, Hu Y, Zhou X (2014) Flock house virus RNA polymerase initiates RNA synthesis de novo and possesses a terminal nucleotidyl transferase activity. PLoS One 9: e86876
Google Scholar: Author Only Title Only Author and Title

Yu S, Kim VN (2020) A tale of non-canonical tails: gene regulation by post-transcriptional RNA tailing. Nat Rev Mol Cell Biol 21: 542–556

Google Scholar: Author Only Title Only Author and Title

Yuan X, Shi K, Simon AE (2012) A local, interactive network of 3' RNA elements supports translation and replication of Turnip crinkle virus. J Virol 86: 4065–4081

Google Scholar: Author Only Title Only Author and Title

Zhang W, Murphy C, Sieburth LE (2010) Conserved RNaseII domain protein functions in cytoplasmic mRNA decay and suppresses Arabidopsis decapping mutant phenotypes. Proc Natl Acad Sci USA 107: 15981–15985

Google Scholar: Author Only Title Only Author and Title

Zhao Y, Yu Y, Zhai J, Ramachandran V, Dinh TT, Meyers BC, Mo B, Chen X (2012) The Arabidopsis nucleotidyl transferase HESO1 uridylates unmethylated small RNAs to trigger their degradation. Curr Biol 22: 689–694

Google Scholar: Author Only Title Only Author and Title

Zhu HY, Ling KS, Goszczynski DE, McFerson JR, Gonsalves D (1998) Nucleotide sequence and genome organization of grapevine leafroll-associated virus-2 are similar to beet yellows virus, the closterovirus type member. J Gen Virol 79 (Pt 5): 1289–1298

Google Scholar: Author Only Title Only Author and Title

Zigáčková D, Vaňáčová Š (2018) The role of 3' end uridylation in RNA metabolism and cellular physiology. Philos Trans R Soc Lond, B, Biol Sci 373: 20180171

Google Scholar: Author Only Title Only Author and Title

Zuber H, Scheer H, Ferrier E, Sement FM, Mercier P, Stupfler B, Gagliardi D (2016) Uridylation and PABP cooperate to repair mRNA deadenylated ends in Arabidopsis. Cell Rep 14: 2707–2717

Google Scholar: Author Only Title Only Author and Title

Zuber H, Scheer H, Joly A-C, Gagliardi D (2018) Respective contributions of URT1 and HESO1 to the uridylation of 5′ fragments produced from RISC-cleaved mRNAs. Front Plant Sci 9: 1438

Google Scholar: Author Only Title Only Author and Title